14. Wang GJ, Volkow ND, Wolf AP, Brodie JD, Hitzemann RJ. Intersubject variability of brain glucose metabolic measurements in young normal males. J Nucl Med 1994;35:1457–1466.
15. Arahata Y, Hirayama M, Ieda T, et al. Parieto-occipital glucose hypometabolism in Parkinson's disease with autonomic failure. J Neurol Sci 1999;163:119–126.
16. Hutchins GD, Holden JE, Koeppe RA, Halama JR, Gatley SJ, Nickles RJ. Alternative approach to single-scan estimation of cerebral glucose metabolic rate using glucose analogs, with particular application to ischemia. J Cereb Blood Flow Metab 1984; 4:35–40.
17. Eberling JL, Richardson BC, Reed BR, Wolfe N, Jagust WJ. Cortical glucose metabolism in Parkinson's disease without dementia. Neurobiol Aging 1994;15:329–335.
18. Bohnen NI, Minoshima S, Giordani B, Frey KA, Kuhl DE. Motor correlates of occipital glucose hypometabolism in Parkinson's disease without dementia. Neurology 1999;52:541–546.
19. Hu MTM, Taylor-Robinson SD, Chaudhuri KR, et al. Cortical dysfunction in non-demented Parkinson's disease patients: a combined (31)P-MRS and (18)FDG-PET study. Brain 2000;123:340–352.
20. Mentis MJ, McIntoshi AR, Perrine K, et al. Relationships among the metabolic patterns that correlate with mnemonic, visuospatial, and mood symptoms in Parkinson's disease. Am J Psychiatry 2002;159:746–754.
21. Goldman-Rakic PS. Cellular basis of working memory. Neuron 1995;14:477–485.
22. Cabeza R, Nyberg L. Imaging cognition II: an empirical review of 275 PET and fMRI studies. J Cogn Neurosci 2000;12:1–47.
23. MacDonald AW III, Cohen JD, Stenger VA, Carter CS. Dissociating the role of the dorsolateral prefrontal and anterior cingulate cortex in cognitive control. Science 2000;288:1835–1838.
24. Hasegawa I, Fukushima T, Ihara T, Miyashita Y. Callosal window between prefrontal cortices: cognitive interaction to retrieve long-term memory. Science 1998;281:814–818.
25. Tomita H, Ohbayashi M, Nakahara K, Hasegawa I, Miyashita Y. Top-down signal from prefrontal cortex in executive control of memory retrieval. Nature 1999;401:699–703.
26. Kretshmann HJ, Weinirich W. Visual systems. In: Cranial neuroimaging and clinical neuroanatomy. New York: Thieme; 1992. p 289–299.
27. Roland PE. The posterior division of the brain: the parietal, temporal, and occipital cortices. In: Brain activation. New York: Wiley-Liss; 1993. p 365–393.
28. Vaphiades MS, Celesia GG, Brigell MG. Positive spontaneous visual phenomena limited to the hemianopic field in lesions of central visual pathways. Neurology 1996;47:408–417.
29. Lawrie SM, Buechel C, Whalley HC, Frith CD, Friston KJ, Johnston EC. Reduced frontotemporal functional connectivity in schizophrenia associated with auditory hallucinations. Biol Psychiatry 2002;51:1008–1001.
30. Manford M, Andermann F. Complex visual hallucinations. Clinical and neurobiological insights. Brain 1998;121:1819–1840.

J Neurosurg 100:679–687, 2004

Long-term stimulation of the subthalamic nucleus in hemiparkinsonian rats: neuroprotection of dopaminergic neurons

SATOSHI MAESAWA, M.D., YOSHIKI KANEOKE, M.D., YASUKAZU KAJITA, M.D., NAOTAKA USUI, M.D., NOBUAKI MISAWA, PH.D., ATSUO NAKAYAMA, M.D., AND JUN YOSHIDA, M.D.

Department of Neurosurgery and Pathology of Biological Response, Nagoya University School of Medicine; and Department of Integrative Physiology, National Institution for Physiological Sciences, Okazaki National Research Institutes, Okazaki City, Japan

Object. The goal of this study was to evaluate the neuroprotective effects conferred by long-term electrical stimulation of the subthalamic nucleus (STN) against degeneration of dopaminergic neurons by assessing motor functional and immunohistological findings in hemiparkinsonian rats.

Methods. In 13 of 25 rats, a concentric microelectrode was stereotactically implanted into the right STN under the guidance of extracellular microelectrode recording. After this had been done the animals were given an injection of 6-hydroxydopamine (6-OHDA) into the right striatum. Seven of the rats received continuous stimulation (frequency 130 Hz, intensity 80–100 μA) for 2 weeks (Group A); the other six did not receive any stimulation during this period (Group B). Twelve rats did not receive electrode implantation and underwent 6-OHDA injection only; these animals served as a control group (Group C). After 2 weeks, motor function in the rats was evaluated by conducting an amphetamine-induced rotation test. Finally, tyrosine hydroxylase–immunoreactive neurons in the pars compacta of the substantia nigra (SNc) were counted to evaluate the extent of degeneration of dopaminergic neurons. Ipsilateral rotation was significantly decreased in Group A, regardless of the effects of stimulation delivered during the test ($p < 0.05$). Rats in Group B demonstrated typical circling as did those in Group C, except that on stimulation Group B rats immediately stopped circling or changed direction. Tyrosine hydroxylase–immunoreactive neurons in the SNc were significantly preserved in the animals in Group A, whereas neurons in animals in Groups B and C were moderately depleted ($p < 0.01$).

Conclusions. Acutely, STN stimulation improved rotation symmetry in rats with moderate SNc degeneration. When STN stimulation had been applied for the preceding 2 weeks, motor function was better and SNc neural degeneration was significantly milder. Subthalamic nucleus stimulation thus appears to protect dopaminergic neurons in this hemiparkinsonian model, in addition to improving motor function in these animals.

KEY WORDS • **deep brain stimulation** • **Parkinson disease** • **neuroprotection** • **subthalamic nucleus** • **6-hydroxydopamine** • **rat**

DEEP brain stimulation directed to the STN is a promising surgical treatment for advanced PD, which is in use at many institutions worldwide.[8] This treatment can decrease motor symptoms of the disease such as rigidity, bradykinesia, tremor, and drug-induced dyskinesia. In addition to alleviation of motor symptoms, possible neuroprotective effects of DBS of the STN are now suspected.[7,26–28] The underlying hypothesis is that STN DBS or ablation can decrease glutamate-induced excitotoxicity,[21] which is induced by the STN on the SNc. Any proven neuroprotective effects of DBS or ablation of the STN would assign to these modalities an important role in the arrest or delay of the progression of PD and expand the indications for these treatments to include moderate or early disease stages.

Recent preclinical research has addressed this issue.[7,26–28] Authors of some reports have concluded that STN ablation in rats prevents further degeneration of dopaminergic neurons in the SNc. These studies involved chemical STN ablation rather than stimulation, however, and thus questions remain as to whether STN stimulation itself also can act neuroprotectively. Furthermore, controversy persists regarding whether the clinical effectiveness of DBS has the same mechanism as that underlying the benefits conferred by ablation.[1,2,9,11,12,33,34] One problem in resolving the matter has been the lack of a reliable long-term STN DBS model in awake rats. To overcome this obstacle, we have developed a technique of DBS of the STN in awake rats and have used it in an established rat model of PD (6-OHDA–induced nigrostriatal degeneration).[6,25] Our purpose was to evaluate the neuroprotection conferred by long-term DBS of the STN as well as its effects on motor function and to consider the implications of this method's mechanisms of therapeutic effects.

Abbreviations used in this paper: ANOVA = analysis of variance; AP = anteroposterior; DBS = deep brain stimulation; DV = dorsoventral; GABA = γ-aminobutyric acid; ML = mediolateral; 6-OHDA = 6-hydroxydopamine; PD = Parkinson disease; PLSD = protected least significant difference; SN = substantia nigra; SNc = pars compacta of the SN; SNr = pars reticulata of the SN; STN = subthalamic nucleus; TH = tyrosine hydroxylase; VPM = ventral posteriomedial (thalamic) nucleus; ZI = zona incerta.

TABLE 1

Treatment protocol for the experimental groups

Factor	Group A	Group B	Group C
no. of rats	7	6	12
DBS electrode implanted in STN	yes	yes	no
continuous stimulation of STN	yes	no	no
6-OHDA injection	yes	yes	yes

Materials and Methods

Animal Preparation

Twenty-nine Sprague–Dawley rats were initially prepared for this study. In four of them a histological study showed an unsatisfactory location of the stimulation electrode and those animals were excluded (detailed information on the location of each electrode is described in *Results*). Consequently, 25 rats were included in this study. The rats, which weighed between 245 and 275 g each, were housed in a temperature-controlled environment at 24°C with a 12-hour light/dark cycle and were given free access to food and water. All animal experiments were performed in accordance with the *Guidelines for Animal Experimentation of Nagoya University*, which were issued in April 2000.

Overview of the Experimental Design

The rats were divided into three groups. In Group A (seven rats), a DBS electrode was stereotactically implanted into the right STN with the guidance of microelectrode recordings. On the next day, the rats were observed during a brief stimulation at various intensities to determine the optimal intensity for long-term stimulation (therapeutic intensity) for each rat. Two days after implantation, 6-OHDA was stereotactically injected into the right striatum to produce hemiparkinsonism. Subthalamic nucleus stimulation at the therapeutic intensity was begun immediately after the 6-OHDA injection and continued for 2 weeks. In Group B (six rats) the animals underwent DBS electrode implantation into the STN followed by an injection of 6-OHDA, but they did not receive long-term stimulation. This group was used to evaluate the pathological changes in the SNc as a sham surgical group and also to examine motor responses to amphetamine with and without acute stimulation; they represented rats with considerable nigrostriatal dopaminergic neuronal degeneration. In Group C (12 rats) the animals underwent only the 6-OHDA injection into the right striatum and served as a control group. Two weeks after 6-OHDA administration, the rats in all three groups were examined in an amphetamine-induced rotation test. After this test the animals were killed and their brains were examined histopathologically. The characteristics of each group are summarized in Table 1. Detailed methods for each step of the protocol are described later in this paper.

Microelectrode Recording and DBS Electrode Implantation

Each rat was anesthetized by an intraperitoneal injection of chloral hydrate (400 mg/kg). Afterward, the head was secured in a stereotactic frame (David Kopf Instruments, Tujunga, CA) and the body temperature of each animal was maintained at 37°C. The incisor bar was set at −3.5 mm to orient the horizontal calvarial surface. An incision was made in the skin at the midline and a small burr hole was drilled in the right posterior skull. The initial target representing the STN was set at a point 2.5 mm lateral to the midline, 3.8 mm posterior to the bregma, and 7.6 mm deep from the surface of the dura mater, according to the atlas of Paxino and Watson.[24] For a precise identification of STN location, we performed extracellular microelectrode recording. A tungsten microelectrode (tip diameter 40 μm) was inserted through the burr hole and aimed at the initial target. Then, it was advanced slowly by using a micromanipulator (Narishige, Tokyo, Japan). Potentials at the electrode were amplified 10,000 times and conducted through a bandpass filter (10–10,000 Hz; Dam 80i; World Precision Instruments, Aston, UK) and monitored with the aid of an oscilloscope display and an audio output. Activities of neurons in various anatomical structures, such as the VPM, ZI, STN, and cerebral peduncle can be distinguished by their characteristic potentials, firing frequencies, and firing patterns. Typical activities of neurons in the VPM, ZI, STN, and SNr are demonstrated in Fig. 1. In the VPM, we typically encountered discrete high-amplitude potentials and burst activity. These thalamic recordings were notable for their heterogeneity, showing different waveforms and firing patterns. The most useful electrical landmark in the VPM was a sensory response. In the ventral portion of the VPM (5–6.5 mm deep with respect to the dura mater), we usually noted these responses when touching the contralateral barba, face, or forepaw. As the electrode was advanced slowly, it entered a relatively silent area, which was consistent with the ZI and measured from 0.5 to 1 mm. When the electrode entered the STN, the number of spikes suddenly increased. The typical activity of neurons in the STN was characterized by an irregular firing pattern and a high firing rate (mean frequency 40.9 ± 12.9 Hz). The pattern of STN firing extended for 100 to 200 μm.

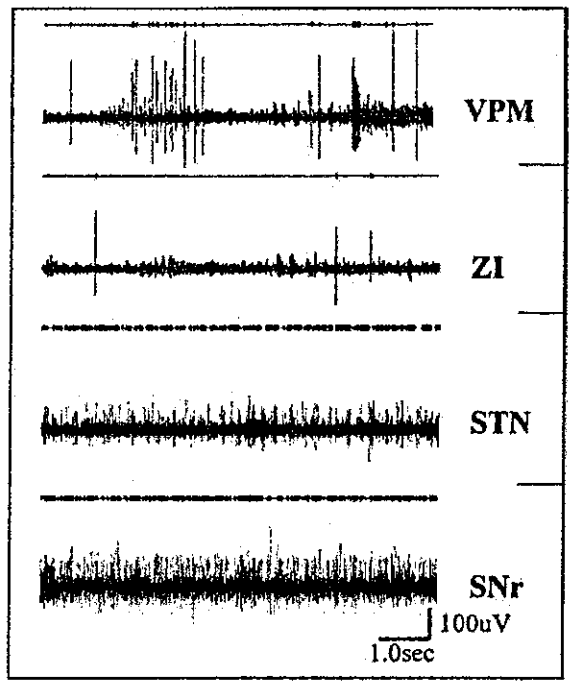

FIG. 1. Tracings of the typical neuron activities in the VPM, ZI, STN, and SNr during microelectrode recording. In the VPM, typical neuron activity was characterized by discrete high-amplitude potentials and burst activity. After the electrode was passed through the silent area (ZI) and into the STN, an irregular firing pattern and a high firing rate were observed (40.9 ± 12.9 Hz). If the electrode was placed too far posteriorly, we encountered SNr neuron activity, which demonstrated a frequent, high-amplitude, and irregular pattern, resembling that in the STN, although the frequency of neuronal firing in the SNr is usually higher than that observed in the STN (68.3 ± 8.6 Hz).

After passing through the STN, the electrode usually entered the cerebral peduncle, where the recording was strikingly silent. When high-frequency neuron activities extended farther than 300 μm, the electrode position was likely to be too posterior and probably within the SNr. In the SNr neuron activity is manifested by frequent, high-amplitude, and irregular patterns, resembling that in the STN. Although the frequency of neuron firing in the SNr is usually higher than that in the STN, with sparser neuron activities (mean frequency 68.3 ± 8.6 Hz), distinction was difficult. In such a situation, we moved the electrode 100 to 200 μm anterior and resumed recording. After electrophysiologically confirming the target, we implanted the

DBS electrode at the same position. This electrode was a bipolar concentric microelectrode with a tip diameter of 100 μm, a shaft diameter of 200 μm, and had a distance between its two contacts of 100 μm (Unique Medical, Osaka, Japan). The electrode configuration is shown in Fig. 2A. After implantation, the electrode was affixed to the skull with dental cement. Stimuli were delivered by a biphasic stimulus isolator (BAK Electronics, Mount Airy, MD), connected to the stimulating electrode. To allow the rats to move freely while under continuous stimulation and to prevent mechanical interference with the lead connection, each rat was housed in a cage designed to permit movement.[16]

Evaluation of the Behavioral Response to DBS of the STN

One day after the rats underwent implantation of the DBS electrode, each rat in Group A was stimulated at various intensities for a short period (30 seconds–5 minutes) and the behavioral response was evaluated. Only the stimulus intensity was varied from 25 to 600 μA; all other parameters remained fixed at a frequency of 130 Hz and a pulse duration of 60 μsec. The purpose of this evaluation was to determine the optimal intensity for long-term stimulation (therapeutic intensity) in each rat. In general, when the intensity increased, each rat responded with involuntary movements that ranged from minor to major. The maximum intensity that did not cause such involuntary movements was chosen as the therapeutic intensity.

Administration of 6-OHDA

Two days after implantation of the DBS electrodes, 6-OHDA was administered stereotactically into the right striatum in the two groups of rats in which electrodes had been implanted and in the control group of rats without electrodes. The injection was given in the manner described by Cadet and Zhu.[6] Each rat was anesthetized by an intraperitoneal injection of chloral hydrate (400 mg/kg) and was placed in a stereotactic frame. Each animal received two infusions of 6-OHDA (20 μg in 2 μl of normal saline containing 0.02% ascorbic acid) separated into two sites in the right striatum that corresponded to the following coordinates: AP 1.6 mm, ML 2.4, and DV 4.2; and AP 0.2, ML 2.6, and DV 7. The coordinates were determined according to information contained in the atlas of Paxinos and Watson.[24] The drug was infused slowly at a rate of 1 μl/minute by using a Hamilton syringe. After infusion the needle was kept in place for 5 minutes before its removal.

Amphetamine-Induced Rotation Test

Two weeks after administration of 6-OHDA, amphetamine-induced rotation was tested in all groups. Each rat was placed in an individual cage and given 30 minutes to adapt to this environment. After acclimation, amphetamine was intraperitoneally administered (2.5 mg/kg) to each animal and the rats were observed for the following 60 minutes. The numbers of full clockwise and counterclockwise turns per minute in response to amphetamine injection were recorded. In Groups A and B, both stimulation-on and stimulation-off periods were examined. The first 20-minute period consisted of a stimulation-off period, the next 20-minute period of a stimulation-on period, and the last 20-minute period consisted of a stimulation-off period. During the stimulation-on period, the therapeutic intensity, which had been identified earlier (see *Evaluation of the Behavioral Response to DBS of the STN*) was used for the stimulation. These stimulus intensities ranged from 80 to 100 μA, depending on the individual rat.

Histological Assessment

On the day following motor testing, the rats were deeply anesthetized with chloral hydrate and perfused transcardially with 60 ml of saline followed by 200 ml of 4% paraformaldehyde in phosphate-buffered saline. Their brains were removed and postfixed in the same fixative for 24 hours. The fixed brains were embedded in paraffin and cut into 7-μm-thick coronal sections through the STN, pallidum, and SNc. Each section was stained with H & E prior to a standard histological examination. Sections of SNc were subjected to TH-immunohistochemical analysis. Tyrosine hydroxylase staining was performed following the modified avidin-biotin-peroxidase complex method. Anti-TH rabbit polyclonal antibody (dilution, 1:200; Affiniti Research Products, Ltd., Mamhead, UK) was applied as the primary antibody. The TH-immunoreactive neurons in the SNc were then counted, ordinarily in the section that exhibited the most discrete separation of the SNc from the ventral tegmental area by the optic tract. The ratio of TH-immunoreactive neurons on the right (treated) side to those on the left (intact) side was calculated as a percentage and compared between groups.

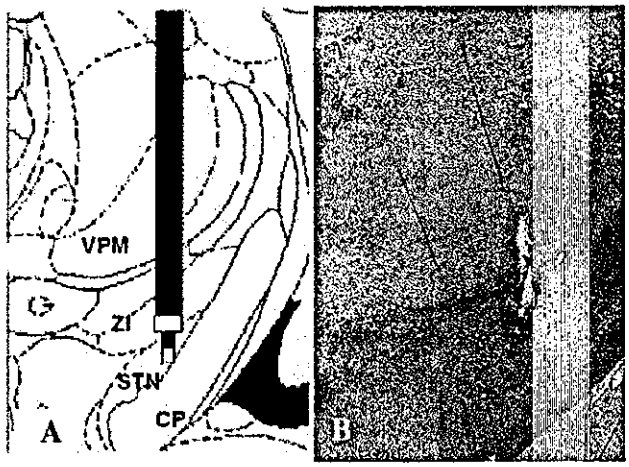

FIG. 2. The stimulating electrode and its placement. A: Schematic diagram adapted from the stereotactic atlas of Paxinos and Watson to show the configuration of the stimulation electrode. (Original figure reprinted from Paxinos W, Watson C: **The Rat Brain in Stereotactic Coordinates**, ed 4, fig. 33, 1997, with permission from Elsevier.) B: Photomicrograph showing a section of brain tissue obtained from the level of the STN. H & E, original magnification × 10. The diameter of the tip of the electrode is 100 μm and that of the shaft is 200 μm, demonstrating that the electrode tip is placed successfully in the STN. CP = cerebral peduncle.

Statistical Analysis

The results are expressed as means ± standard errors of the means. Statistical evaluation was performed using a factorial ANOVA with the Fisher PLSD as a post hoc test. An error probability less than 0.05 was considered significant.

Results

Short-Term Behavioral Response to DBS of the STN

All rats in Groups A and B were evaluated for behavioral responses to STN stimulation 24 hours after implantation. With no or low (< 40 μA) stimulation present, no behavioral changes were apparent, including any clear rotation asymmetry. As the stimulus intensity progressively increased, several stereotypical movements appeared. The characteristics of involuntary movements at various intensities are plotted in Fig. 3. With stimulation at approximately 50 μA, the rats displayed a transient left-sided dyskinetic movement on the side contralateral to the site of implantation. Generally, these occurred in the orofacial area or the forepaw and lasted for less than 1 minute. As the stimulation increased, the rats demonstrated a subtle tendency to turn slightly to the left. When the intensity of the stimulus

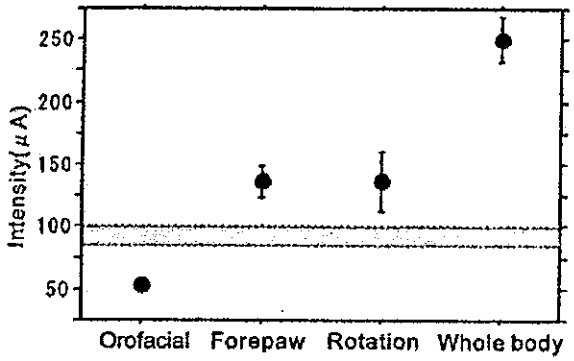

FIG. 3. Graph showing characteristics of involuntary movements at various stimulus intensities. At 50 μA, the animals exhibited transient dyskinetic movement in the contralateral orofacial area. When the stimulus intensity was increased to approximately 120 μA, a dyskinetic movement was apparent in the left forepaw and the rats began to rotate rapidly to the left. At approximately 250 μA, all rats displayed generalized dyskinetic movements. The *gray area* shows the optimal therapeutic intensity for continuous stimulation (80–100 μA).

was increased to approximately 120 μA, the dyskinetic movement was apparent in the left forepaw and the rats began to rotate rapidly to the left. As the stimulation intensified further, the dyskinetic movements extended to the entire body and became severe. With stimulation set at approximately 250 μA, all rats displayed generalized dyskinetic movements and tonic twisting of the body, and they often turned to lie down on their backs. The optimal therapeutic intensity for continuous stimulation was set just below the threshold for apparent dyskinetic movement in the contralateral forepaw, which ranged from 80 to 100 μA. When the rats were continuously stimulated at this therapeutic intensity, a partial diskinetic movement was occasionally seen at the beginning of the stimulation, but soon disappeared. No changes in feeding, external appearance, or locomotion were noted for the following 2 weeks.

Motor Effects of DBS of the STN in Rats New to Long-Term Stimulation

Rats in the control group (Group C) demonstrated circling to the right (ipsilateral to the site of the 6-OHDA injection) after amphetamine administration (6.11 ± 1.19 turns/minute). Rats with implanted electrodes that had not undergone previous continuous stimulation demonstrated a circling behavior similar to that observed in Group C before the stimulation was turned on, although the number of turns (5.23 ± 1.1 turns/minute) was slightly less than that in controls. Immediately after stimulation at the therapeutic intensity (80–100 μA), the rats stopped circling and slightly veered or slowly rotated to the opposite side (−0.51 ± 0.27 turns/minute [left rotations are expressed as minus values]) (Fig. 4 *upper*). Compared with the rotation observed in the control group, or compared with their own rotation with the stimulation turned off, the rotation rate of rats in Group B with stimulation was significantly low (factorial ANOVA with Fisher PLSD, $p = 0.0005$ and $p = 0.0047$) (Fig. 4 *center*). This response was dependent on the intensity of the stimulation. We usually started by setting the therapeutic

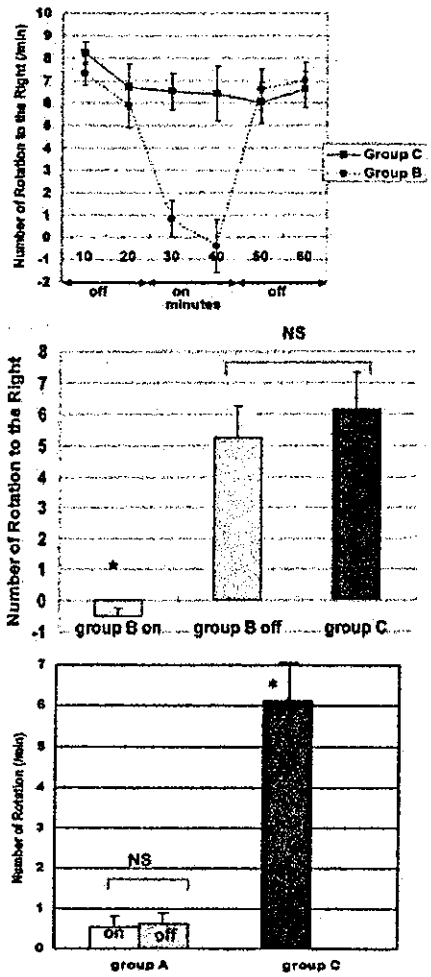

FIG. 4. Motor testing in rats with or without long-term stimulation and in control animals. *Upper:* Plot of results in the amphetamine-induced rotation test over time in Groups B (no constant stimulation) and C (control group). The animals in Group C demonstrated the circling behavior to the right after amphetamine administration. Those in Group B displayed a similar circling behavior without stimulation. Immediately on stimulation the rats in Group B stopped circling and began to veer or rotate somewhat toward the opposite side. *Center:* Bar graph showing a comparison of the results of the amphetamine-induced rotation test in Groups B and C. *Open bar* represents the number of rotations in Group B during stimulation. Rotations to the left are expressed as a minus value. The gray bar represents the number of rotations in Group B with the stimulation turned off. Compared with the number of rotations in the control group or with the number of rotations in their own group when stimulation was turned off, the rotation in Group B rats during stimulation on was significantly lower. *Lower:* Bar graph showing a comparison of the results of the amphetamine-induced rotation test in Groups A and C. The animals in Group A showed no typical circling during either the stimulation-on or stimulation-off periods. The animals in Group C displayed typical circling after amphetamine administration. *Asterisks* represent a significant difference between groups. NS = not significant.

intensity just below the threshold of apparent dyskinetic movement. When the intensity was increased above the threshold, however, the rats rotated increasingly often and rapidly in the direction opposite to the rotation observed

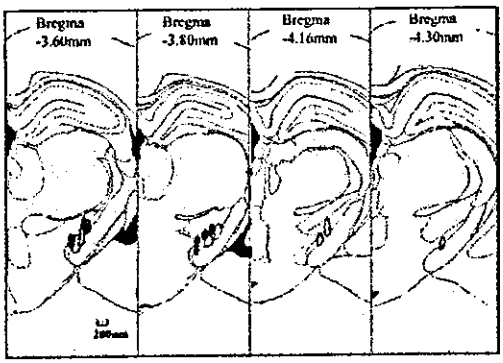

FIG. 5. Locations and sizes of lesions after placement of the stimulation electrodes, determined by the histological analysis and superimposed on figures from the atlas of Paxinos and Watson. Open-circled areas represent lesions observed after a continuous 2-week stimulation in Group A (seven rats). Closed circled areas represent lesions observed without continuous stimulation in Group B (six rats). All lesions are located in the STN (subthalamic nucleus). The size and location of lesions were similar in both groups. (Original figures reprinted from Paxinos W, Watson C: **The Rat Brain in Stereotactic Coordinates,** ed 4, figs. 33, 34, and 35, 1997, with permission from Elsevier.)

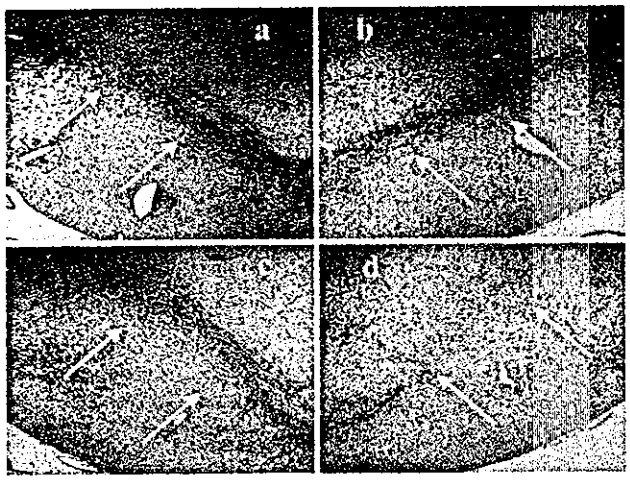

FIG. 6. Photomicrographs of coronal sections illustrating both sides of the SNc in Groups A (a and b) and C (c and d). Compared with the left (intact) side, the right (treated) SNc in Group C rats exhibits a marked depletion of dopaminergic neurons *(arrows)*, whereas in Group A rats the neurons in the right SNc are well preserved. Immunostaining for TH, original magnification × 10.

without stimulation. We did not evaluate these potentially confusing high-intensity results in detail, focusing instead on stimulation at the therapeutic intensity.

Motor Effects of DBS of the STN in Rats Undergoing Long-Term Stimulation

Rats undergoing 2 weeks of continuous stimulation (Group A) displayed no typical circling during the amphetamine-induced rotation test with stimulation turned either on or off (turns/minute: on, 0.54 ± 0.26; off, 0.61 ± 0.28) (Fig. 4 *lower*). Both values were significantly smaller than those obtained in the control group (factorial ANOVA with Fisher PLSD, $p = 0.003$ and $p = 0.004$, respectively). Although the rats rotated toward the injected side several times after administration of amphetamine, this rotation was far from a typical amphetamine-induced rotation in that it was more like ambling than circling. With the stimulation turned on, the rats often ceased their movements, and occasionally turned slightly to the opposite side. These movements seldom attained the appearance of contralateral circling, as seen during stimulation in the animals in Group B.

Localization of DBS of the STN

To identify the location of the STN, we used extracellular microelectrode recording in all rats and targeting usually required fewer than three trajectories (mean 1.4). Although we initially attempted to implant the stimulation electrode in 17 rats in Groups A and B, the sites selected in four rats (23.5%) were unsatisfactory, as shown histopathologically (two electrodes were located too deeply in the cerebral peduncle and the other two were located posteriorly, near the SNr). These four animals were subsequently excluded from the study. The success rate for localization was 76.5% (13 of 17). In these 13 rats, the tip of the implanted electrode was shown histologically to have been situated in the STN. Figure 2B illustrates the electrode location in the STN. We found that a small lesion developed after continuous stimulation in all rats. The locations and sizes of lesions in all the rats in Groups A and B are demonstrated in Fig. 5. We consider the sizes of the lesions to be acceptable because they were only slightly larger than the diameter of the electrode. Even the rats in Group B had lesions of a similar size without continuous stimulation. The mean diameters of the lesions were the following: AP 262 ± 17 μm, ML 278 ± 27 μm, and DV 468 ± 58 μm in Group A; and AP 259 ± 35 μm, ML 263 ± 29 μm, and DV 456 ± 68 μm in Group B. Most important, most STN neurons that were located beyond the lesion showed no remarkable morphological change.

Dopaminergic Neuron Loss in the SNc

Tyrosine hydroxylase–immunoreactive neurons in the ipsilateral SNc were depleted after the 6-OHDA injection in animals in Groups B and C. In contrast, these neurons were well preserved after long-term DBS of the STN (Group A) (Fig. 6). The mean numbers of TH-immunoreactive neurons in the left and right SNc were as follows: Group A, 90.3 ± 13.8 in the left and 76.1 ± 14.1 in the right; Group B, 82.6 ± 10.6 in the left and 38 ± 8.3 in the right; and Group C, 70.3 ± 7.8 in the left and 21.5 ± 5.4 in the right. The ratio of TH-immunoreactive neurons in the right SNc (injected side) to those in the left SNc (intact side) in each group was 84.8 ± 7.6% in Group A, 43.5 ± 4.7% in Group B, and 29.3 ± 5.4% in Group C. The ratio of TH-immunoreactive neurons in the animals in Group B decreased fairly similarly to those in the control group, although the ratio was slightly higher (43.5 ± 4.7% compared with 29.3 ± 5.4%, $p = 0.12$ [not significant]). Meanwhile, the ratio of TH-immunoreactive neurons in Group A was much higher than that measured in other two groups. Differences between Groups A and C, as well as between Groups A and B, were statistically significant ($p = 0.001$ and 0.003, factorial ANOVA followed by Fisher PLSD) (Fig. 7).

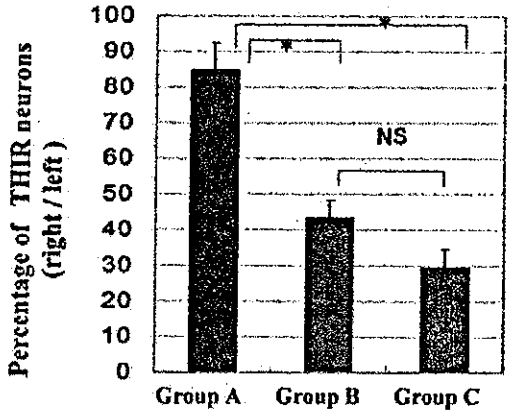

FIG. 7. Bar graph showing the ratio (as a percentage) of TH-immunoreactive (THIR) neurons on the right (treated) side to those on the left (intact) side in the SNc in each group. The TH-immunoreactive neurons in Group B were decreased almost as much as in the control group, although the ratio was slightly higher (43.5 ± 4.7% compared with 29.3 ± 5.4% [p = 0.12]). The ratio of TH-immunoreactive neurons in Group A was significantly higher than in the other groups (84.8 ± 7.6% compared with 29.3 ± 5.4% in the control Group C [p = 0.001] and with 43.5 ± 4.7% in Group B [p = 0.003]). *Asterisks* indicate a significant difference.

Discussion

The results of the present study support our hypothesis that STN stimulation can improve behaviorally evident motor abnormalities and protect nigral dopaminergic neurons from 6-OHDA–induced toxicity. Two main topics will be considered here: our experimental model and the potential neuroprotective effects of DBS of the STN.

Experimental Model for Long-Term DBS of the STN

In this study we applied long-term DBS to the STN in a rat model that was designed to permit observation of awake animals during continuous stimulation of the STN. Two aspects of our model are unique. The first was the technique used to identify the location of the STN. In previous studies[5,7,10,12,17,18,26,27,30,34] investigators only used stereotactic methods according an atlas; however, placing the tip of the stimulating electrode precisely in the STN is technically difficult: the horizontal extension of the STN is at most 200 μm and the distance between the two contacts of the stimulating electrode in the STN is 100 μm. We therefore used extracellular microelectrode recording in combination with conventional stereotaxy to provide targeting guidance. The recording electrode was inserted along a horizontal line with the STN located between the ZI and the cerebellar peduncle. Firing of neurons in the STN could be distinguished fairly easily because the STN demonstrated high-frequency, irregular firing patterns, whereas the ZI and the cerebellar peduncle were relatively silent. This method was very helpful for accurate targeting in this experiment. In fact, more than half of the attempts at localization were unsuccessful without microelectrode recording in our pilot study, whereas after using electrophysiological guidance the success rate for localization virtually improved to 76.5% (13 of 17 rats).

Second, a special consideration was given to optimal stimulation parameters. Benazzouz and colleagues[2,3] studied electrophysiologically the firing rates of neurons in the globus pallidus and SNr in response to DBS of the STN in anesthetized rats. The parameters of stimulation examined in that study were a frequency of 1 to 1000 Hz, a pulse width of 60 μsec, and an intensity ranging between 100 and 1000 μA. These authors concluded that most SNr neurons that were tested (91%) presented significant suppression of neuron activity in response to high-frequency stimulation delivered to the STN with parameters of 130 Hz frequency and 300 μA intensity. In other electrophysiological or microdialysis studies, similar parameters were used (frequency 130 Hz, pulse width 60 μsec, and intensity range 300–1000 μA).[3,5,17,18,20,23,34] Considering these data, we initially assumed that a high frequency such as 130 Hz should be used; its effectiveness has been proven in animal studies and seen clinically in patients with PD. With regard to the optimal stimulation intensity in the awake rat, however, we could not obtain guidance from previous reports. In a preliminary study, we initially used an intensity greater than 300 μA, but saw a high incidence of severe and extensive dyskinetic movements. We assumed that these dyskinetic movements resembled abnormal involuntary movements, which were sometimes provoked by inappropriate stimulation in humans.[15] Furthermore, we assumed that some rats receiving such high-intensity stimulation exhibited severe destruction in the STN and surrounding tissues. We concluded that a difference existed between the stimulation intensities, causing behavioral changes in awake rats, and intensities that cause changes that are only apparent electrophysiologically in the anesthetized rats. We therefore decided to use a relatively low intensity, which was determined by the essential absence of behavioral phenomena caused by stimulation (80–100 μA). In fact, with continuous stimulation at this "therapeutic intensity," no rat exhibited changes in feeding, external appearance, or locomotion during 2 weeks of observation. Furthermore, all rats in Group B exhibited an immediate decrease in amphetamine-induced circling in response to stimulation at this therapeutic intensity. Thus, we believed that the stimulus intensity that we selected was suitable for our study. Altogether, our model of DBS of the STN enabled us to evaluate behavioral changes during long-term stimulation and to analyze the motor and neuroprotective benefits conferred by long-term stimulation. We believe that this model will prove to be useful for further studies related to DBS, including treatment in combination with neurotrophic factors or neuronal transplantation, or possibly in assessing new treatments for epilepsy.[4,10,19,29,31]

Neuroprotective Effects of DBS of the STN

We placed the DBS electrode into the STN before delivery of the 6-OHDA insult; therefore, considerable controversy surrounds the justification of the experimental design for neuroprotection, with regard to the timing of treatment. Nevertheless, this "pretreatment design" has been used often in previous research on neuroprotection, mainly because the neurotoxic process of 6-OHDA could be completed in the very early phase after administration.[4,7,10,19,26,27,29] Certainly, further evaluation should be performed using a more sophisticated experimental design; however, it is significant-

ly important to demonstrate neuroprotective effects in this commonly used design as the first step.

In this study, the neuroprotective effect on dopaminergic neurons in the SNc due to long-term DBS of the STN was demonstrated by the circling behavior of the rats and the immunohistochemical data. Although some reports have presented similar immunohistochemical results after STN lesioning by kainic acid or ibotenic acid,[7,26,27] our study is the first to demonstrate these data as they relate to DBS of the STN in awake hemiparkinsonian rats. In rats that underwent electrode implantation in the STN without continuous stimulation (Group B), nearly as many SNc neurons were lost as a result of the striatal 6-OHDA injection as in control animals, whereas in rats that received STN stimulation continuously for 2 weeks (Group A) the SNc neurons were protected from this insult. Although a small lesion developed after continuous stimulation, the size of the lesion was similar to that in the noncontinuously stimulated rats in Group B, in which the loss of dopaminergic neurons was equivalent to that in controls, and we therefore concluded that long-term stimulation was necessary to protect the SNc neurons. The results of the amphetamine-induced rotation test correlated well with the immunohistochemical findings. We assumed that the reason why rats in Group A did not display typical circling behavior after amphetamine administration, irrespective of stimulation during the test, was that the SNc dopaminergic neurons on the treated side were sufficiently preserved to prevent or minimize a drug-induced abnormality in rotation. On the other hand, the rats in Group B displayed typical circling behavior before the stimulation was given. Apparently, their SNc dopaminergic neurons were compromised to an extent, causing rotation asymmetry. Acute stimulation immediately reversed the asymmetry. This result paralleled the clinical observation that DBS of the STN can improve major motor symptoms in patients with PD immediately after stimulation. Recently, Meissner and associates[17] showed similar changes in amphetamine-induced rotation behavior after DBS of the STN in awake rats. In addition, by using microdialysis they showed increased dopamine metabolism in the striatum during acute stimulation. Thus, an immediate response in Group B of our study can be explained by an immediate increase in striatal dopamine after stimulation.

Although controversy persists as to whether DBS inhibits its neuronal activity in the stimulated structure and, consequently, decreases output from it, our results fit a hypothesis that DBS decreases output from the STN that is directed to the SN. We offer one possible explanation of our results for both motor improvement and neuroprotection of SNc dopaminergic neurons in the following paragraph and Fig. 8.

In PD or in 6-OHDA–induced nigrostriatal degeneration, the neurons in the STN and the SNr are hyperactive, whereas the neurons in the SNc are strongly suppressed by GABAergic control from the SNr.[1,2,20] Major STN output pathways include glutaminergic excitatory fibers to the SNr, with some fibers reaching the SNc through the SNr.[22] With the hyperactivity of the STN suppressed by DBS of the STN, excessive excitation of the SNr is suppressed and SNc neurons are activated as a result. Residual dopaminergic neurons in the SNc then release dopamine to the striatum, causing an immediate improvement in rotation symmetry. This is supported by microdialysis studies in which increased striatal dopamine metabolism after STN DBS has

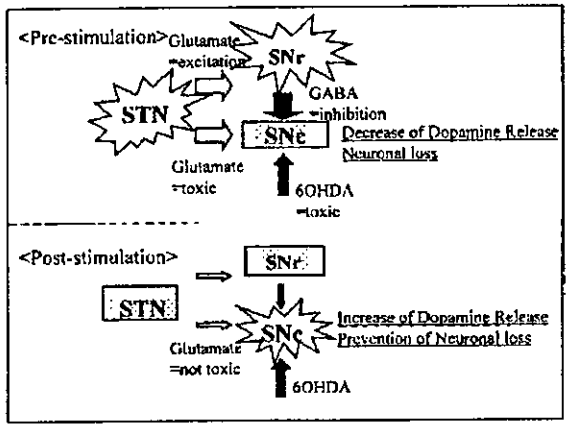

FIG. 8. A schematic diagram showing the hypothesis for the neuroprotection granted by STN stimulation. *Black arrows* represent inhibitory connections and *white arrows* represent excitatory connections. *Upper:* Before stimulation, neurons in the STN and the SNr are hyperactive, whereas neurons in the SNc are suppressed by GABAergic control from the SNr. Excessive glutamate from an excessively activated STN has a neurotoxic effect, resulting in further degeneration of dopaminergic neurons in the SNc. *Lower:* After stimulation, the hyperactivity of neurons in the STN is suppressed, excessive excitation in the SNr is suppressed, and SNc neurons are activated as a result. Residual dopaminergic neurons in the SNc then release dopamine to the striatum, causing an immediate improvement in rotation symmetry. Because excessive glutamate output from the STN is reduced and intracellular metabolism in the SNc is increased, glutamate is relatively less neurotoxic, and dopaminergic neurons in the SNc are preserved from further degeneration.

been demonstrated.[5,17,18,23,30] In some clinical studies decreases in the dose of levodopa were possible after initiating DBS of the STN in patients with PD,[14,32] implying increased dopamine metabolism. On the other hand, excessive glutamate exerts neurotoxic effects via the *N*-methyl-D-aspartate receptor, especially when intracellular metabolism is suppressed in target cells.[21,28] After injection of 6-OHDA, metabolism in the SNc neurons is thought to be strongly suppressed by the retrograde neurotoxic effects of 6-OHDA, reflecting damage to the mithochondrial electron transport system. In this circumstance, excessive glutamate from an excessively activated STN will have a neurotoxic effect, resulting in further degeneration of dopaminergic neurons in the SNc. With DBS of the STN, hyperactivity in the STN is suppressed and excessive glutamate output is thus reduced. Furthermore, stimulation decreases GABAergic input to the SNr and therefore suppression of SNc neuronal activity by the SNr is decreased, increasing neural activity and intracellular metabolism in the SNc. The excessive glutamate is relatively less neurotoxic and dopaminergic neurons in the SNc are preserved from further degeneration.

Some recent reports have concluded that DBS of the STN does not suppress neuronal activities in the internal segment of the globus pallidus or in the SNr, and might not increase dopamine metabolism in the striatum.[13,33,34] Vitek[33] and Hashimoto, et al.,[11] have mentioned that benefits from DBS of the STN cannot be simply explained by excitation or inhibition and that alteration of neuronal firing patterns should be considered. Hilker and colleagues[13] recently re-

ported that according to a positron emission tomography study in which a dopamine D2/3 receptor ligand, [^{11}C]raclopride, was used, patients with PD who were treated with DBS of the STN showed no significant difference between stimulation-on and stimulation-off conditions. If DBS of the STN does not suppress output from the STN, motor improvement and neuroprotective effects are difficult to explain in terms of neurotransmitters and consideration of other mechanisms is required. The effects of acute and continuous stimulation on neurotransmitters may differ. Rather than reflecting a decrease in glutamate neurotoxicity, neuroprotection in the SNc might simply involve a decrease in 6-OHDA uptake by nerve terminals in the striatum, which is induced by unknown effects of DBS of the STN. To determine the true mechanism, further studies are necessary. Microdialysis evaluation of various neurotransmitters during long-term stimulation in our model therefore should be of great interest.

Conclusions

The present study showed immunohistologically and behaviorally that DBS of the STN could prevent further degeneration and dysfunction of SNc neurons in a rat model of PD. This finding may have important implications for the further development of neuroprotective therapeutic strategies. One hypothesis that could explain neuroprotection would involve suppression of glutamate input to the SNc from a hyperactivated STN. Further studies including microdialysis may cast important light on this issue. In addition, the rat model of long-term DBS of the STN used in the current study is reasonably convenient and highly useful for evaluation during continuous stimulation in awake rats. We believe that this model can contribute importantly to future experiments concerning DBS of the STN.

References

1. Benabid AL, Benazzous A, Pollak P: Mechanisms of deep brain stimulation. **Mov Disord 17 (Suppl 3)**:S73–S74, 2002
2. Benazzouz A, Gao DM, Ni ZG, et al: Effect of high-frequency stimulation of the subthalamic nucleus on the neuronal activities of the substantia nigra pars reticulata and ventrolateral nucleus of the thalamus in the rat. **Neuroscience 99**:289–295, 2000
3. Benazzouz A, Hallett M: Mechanism of action of deep brain stimulation. **Neurology 55 (Suppl 6)**:S13–S16, 2000
4. Bowenkamp KE, Lapchak PA, Hoffer BJ, et al: Intracerebroventricular glial cell line-derived neurotrophic factor improves motor function and supports nigrostriatal dopamine neurons in bilaterally 6-hydroxydopamine lesioned rats. **Exp Neurol 145**:104–117, 1997
5. Bruet N, Windels F, Bertrand A, et al: High frequency stimulation of the subthalamic nucleus increases the extracellular contents of striatal dopamine in normal and partially dopaminergic denervated rats. **J Neuropathol Exp Neurol 60**:15–24, 2001
6. Cadet JL, Zhu SM: The intrastriatal 6-hydroxydopamine model of hemiparkinsonism: quantitative receptor autoradiographic evidence of correlation between circling behavior and presynaptic as well as postsynaptic nigrostriatal markers in the rat. **Brain Res 595**:316–326, 1992
7. Carvalho GA, Nikkhah G: Subthalamic nucleus lesions are neuroprotective against terminal 6-OHDA-induced striatal lesions and restore postural balancing reactions. **Exp Neurol 171**:405–417, 2001
8. The Deep-Brain Stimulation for Parkinson's Disease Study Group: Deep-brain stimulation of the subthalamic nucleus or the pars interna of the globus pallidus in Parkinson's disease. **N Engl J Med 345**:956–963, 2001
9. Dostrovsky JO, Lozano AM: Mechanisms of deep brain stimulation. **Mov Disord 17 (Suppl 3)**:S63–S68, 2002
10. During MJ, Kaplitt MG, Stern MB, et al: Subthalamic GAD gene transfer in Parkinson disease patients who are candidates for deep brain stimulation. **Hum Gene Ther 12**:1589–1591, 2001
11. Hashimoto T, Elder CM, Okun MS, et al: Stimulation of the subthalamic nucleus changes the firing pattern of pallidal neurons. **J Neurosci 23**:1916–1923, 2003
12. Henderson JM, Annett LE, Ryan LJ, et al: Subthalamic nucleus lesions induce deficits as well as benefits in the hemiparkinsonian rat. **Eur J Neurosci 11**:2749–2757, 1999
13. Hilker R, Voges J, Ghaemi M, et al: Deep brain stimulation of the subthalamic nucleus does not increase the striatal dopamine concentration in parkinsonian humans. **Mov Disord 18**:41–48, 2003
14. Katayama Y, Kasai M, Oshima H, et al: Subthalamic nucleus stimulation for Parkinson disease: benefits observed in levodopa-intolerant patients. **J Neurosurg 95**:213–221, 2001
15. Limousin P, Pollak P, Hoffmann D, et al: Abnormal involuntary movements induced by subthalamic nucleus stimulation in parkinsonian patients. **Mov Disord 11**:231–235, 1996
16. Matsumura H, Kinoshita G, Satoh S, et al: A novel apparatus that permits multiple routes for infusions and body-fluid collections in a freely-moving animal. **J Neurosci Methods 57**:145–149, 1995
17. Meissner W, Harnack D, Paul G, et al: Deep brain stimulation of subthalamic neurons increases striatal dopamine metabolism and induces contralateral circling in freely moving 6-hydroxydopamine-lesioned rats. **Neurosci Lett 328**:105–108, 2002
18. Meissner W, Reum T, Paul G, et al: Striatal dopaminergic metabolism is increased by deep brain stimulation of the subthalamic nucleus in 6-hydroxydopamine lesioned rats. **Neurosci Lett 303**: 165–168, 2001
19. Natsume A, Mata M, Goss J, et al: Bcl-2 and GDNF delivered by HSV-mediated gene transfer act additively to protect dopaminergic neurons from 6-OHDA-induced degeneration. **Exp Neurol 169**:231–238, 2001
20. Ni ZG, Bouali-Benazzouz R, Gao DM, et al: Time-course of changes in firing rates and firing patterns of subthalamic nucleus neuronal activity after 6-OHDA-induced dopamine depletion in rats. **Brain Res 899**:142–147, 2001
21. Novelli A, Reilly JA, Lysko PG, et al: Glutamate becomes neurotoxic via the N-methyl-D-aspartate receptor when intracellular energy levels are reduced. **Brain Res 451**:205–212, 1988
22. Parent A, Hazrati LN: Functional anatomy of the basal ganglia. II. The place of subthalamic nucleus and external pallidum in basal ganglia circuitry. **Brain Res Brain Res Rev 20**:128–154, 1995
23. Paul G, Reum T, Meissner W, et al: High frequency stimulation of the subthalamic nucleus influences striatal dopaminergic metabolism in the naive rat. **Neuroreport 11**:441–444, 2000
24. Paxinos W, Watson C: **The Rat Brain in Stereotactic Coordinates, ed 4.** San Diego: Academic Press, 1997
25. Perese DA, Ulman J, Viola J, et al: A 6-hydroxydopamine-induced selective parkinsonian rat model. **Brain Res 494**:285–293, 1989
26. Piallat B, Benazzouz A, Benabid AL: Neuroprotective effect of chronic inactivation of the subthalamic nucleus in a rat model of Parkinson's disease. **J Neural Transm Suppl 55**:71–77, 1999
27. Piallat B, Benazzouz A, Benabid AL: Subthalamic nucleus lesion in rats prevents dopaminergic nigral neuron degeneration after striatal 6-OHDA injection: behavioral and immunohistochemical studies. **Eur J Neurosci 8**:1408–1414, 1996
28. Rodriguez MC, Obeso JA, Olanow CW: Subthalamic nucleus-

mediated excitotoxicity in Parkinson's disease: a target for neuroprotection. **Ann Neurol 44 (Suppl 1)**:S175–S188, 1998
29. Rosenblad C, Kirik D, Bjorklund A: Sequential administration of GDNF into the substantia nigra and striatum promotes dopamine neuron survival and axonal sprouting but not striatal reinnervation or functional recovery in the partial 6-OHDA lesion model. **Exp Neurol 161**:503–516, 2000
30. Salin P, Manrique C, Forni C, et al: High-frequency stimulation of the subthalamic nucleus selectively reverses dopamine denervation-induced cellular defects in the output structures of the basal ganglia in the rat. **J Neurosci 22**:5137–5148, 2002
31. Schwarz EJ, Alexander GM, Prockop DJ, et al: Multipotential marrow stromal cells transduced to produce L-DOPA: engraftment in a rat model of Parkinson disease. **Hum Gene Ther 10:** 2539–2549, 1999
32. Vingerhoets FJ, Villemure JG, Temperli P, et al: Subthalamic DBS replaces levodopa in Parkinson's disease: two-year follow-up. **Neurology 58**:396–401, 2002
33. Vitek JL: Mechanisms of deep brain stimulation: excitation or inhibition. **Mov Disord 17 (Suppl 3)**:S69–S72, 2002
34. Windels F, Bruet N, Poupard A, et al: Effects of high frequency stimulation of subthalamic nucleus on extracellular glutamate and GABA in substantia nigra and globus pallidus in the normal rat. **Eur J Neurosci 12**:4141–4146, 2000

Manuscript received May 13, 2003.
Accepted in final form December 17, 2003.
This study was supported in part by the Uehara Memorial Foundation. Portions of this work were presented at the annual meeting of the Congress of Neurological Surgeons, Denver, Colorado, October 2003.

Address reprint requests to: Satoshi Maesawa, M.D., Department of Neurosurgery, Nagoya University School of Medicine, 65, Tsurumai-cho, Showa-ku, Nagoya 466-8550, Japan. email: maesawa@med.nagoya-u.ac.jp.

Quantification of Human Nicotinic Acetylcholine Receptors with ^{123}I-5IA SPECT

Marcelo Mamede, MD, PhD[1]; Koichi Ishizu, MD, PhD[1]; Masashi Ueda, MS[2]; Takahiro Mukai, PhD[1]; Yasuhiko Iida, PhD[2]; Hidenao Fukuyama, MD, PhD[3]; Tsuneo Saga, MD, PhD[1]; and Hideo Saji, PhD[2]

[1]*Department of Nuclear Medicine and Diagnostic Imaging, Graduate School of Medicine, Kyoto University, Kyoto, Japan;* [2]*Department of Patho-Functional Bioanalysis, Graduate School of Pharmaceutical Science, Kyoto University, Kyoto, Japan; and* [3]*Brain Function Imaging Division, Human Brain Research Center, Graduate School of Medicine, Kyoto University, Kyoto, Japan.*

Neuronal nicotinic acetylcholine receptors (nAChRs) are widely distributed in the human brain, especially the $\alpha_4\beta_2$ subtype of nAChR. The cholinergic systems have roles in various neurophysiologic functions, such as learning, memory, and cognition, whereas normal aging and neurodegenerative diseases have been associated with changes in nAChRs. Recently, 5-iodo-3-(2(S)-azetidinylmethoxy)pyridine (5IA) has been synthesized as a radioligand for imaging nAChRs with SPECT. ^{123}I-5IA shows higher affinity toward the nAChR $\alpha_4\beta_2$ subtype, enhanced receptor subtype selectivity, good safety, and low nonspecific binding. **Methods:** In this study, a SPECT quantitative study of human nAChRs binding with ^{123}I-5IA was conducted in healthy volunteers. An arterial input function was obtained for each subject and a 2-compartment model was used to determine the kinetic parameters of ^{123}I-5IA using data from a 6-h scan. The distribution volume (V_T) (mL/mL), which is related to the number of unoccupied binding sites in the brain, was calculated and values were compared with results of a graphical analysis (Logan plot, V_{LG}). **Results:** Analysis of the unmetabolized compound showed a high parent fraction of ^{123}I-5IA in plasma. The results from the 2-compartment model analysis showed high V_T values for the thalamus; moderate values for the brain stem, cerebellum, and basal ganglia; and low values for the cortical regions. Good agreement was observed between V_T values and results of autoradiographic experiments done in vitro for nAChR density in human brain. A high correlation index was observed between distribution volumes from model and graphical analyses. **Conclusion:** Our results indicated that ^{123}I-5IA SPECT is suitable for the quantification of nAChRs in human brain.

Key Words: 5-^{123}I-iodo-3-(2(S)-azetidinylmethoxy)pyridine; SPECT; nicotinic acetylcholine receptors; human brain; distribution volume; quantitative measurement; Logan plot; compartmental model analysis

J Nucl Med 2004; 45:1458–1470

Received Oct. 30, 2003; revision accepted Mar. 4, 2004.

For correspondence or reprints contact: Koichi Ishizu, MD, PhD, Department of Nuclear Medicine and Diagnostic Imaging, Graduate School of Medicine, Kyoto University, Sakyo, 606-8507, Kyoto, Japan.

E-mail: ishizu@kuhp.kyoto-u.ac.jp

Nicotinic acetylcholine receptors (nAChRs) are widely distributed in mammals, appearing in the central and peripheral nervous systems, neuromuscular junctions, and adrenal glands. The majority of high-affinity nAChRs in the brain are of the $\alpha_4\beta_2$ subtype (*1–5*). It has been reported that cholinergic systems play important roles in various neurophysiologic functions such as learning, memory, and cognition (*2,6*). Normal aging and neurodegenerative diseases (such as Alzheimer's disease and Parkinson's disease) have been associated with changes in nAChRs (*2,7–10*). Furthermore, a dose-dependent increase in the subtype in the brain has been observed in chronic nicotine treatment in animal models (*4,11*). This upregulation was also seen in homogenates of autopsied brain samples from smokers (*12,13*), with a return to control levels after cessation of (−)-nicotine treatment (*14*). These findings suggested that upregulation of the $\alpha_4\beta_2$ subtype of nAChR in the brain plays an important role in tobacco tolerance and dependence (*13*).

Therefore, the development of high-affinity radioligands suitable for in vivo imaging of nAChRs, which can provide valuable information from living subjects at different stages of a disease, and the effects of different drugs in patients with neurodegenerative diseases, as well as the upregulation of nAChRs to baseline levels after cessation of treatment with (−)-nicotine or tobacco use, have been of major interest.

Recently, 5-iodo-3-(2(*S*)-azetidinylmethoxy)pyridine (5IA) has been synthesized as a radioligand for imaging nAChRs with SPECT. This compound exhibits extremely high affinity, high selectivity and specificity for the $\alpha_4\beta_2$ subtype of nAChR, relatively low acute toxicity, and acceptable dosimetry (*15–24*).

In this study, a SPECT quantitative study of human nAChRs with ^{123}I-5IA was performed in healthy volunteers. A compartmental model was used to determine the kinetic parameters of ^{123}I-5IA based on the data for a 6-h scan time. Furthermore, due to the necessity of measuring nAChRs in the human brain with a reasonably short scan time for specific achievements, such as in patients with neurodegenerative diseases, a 90-min scan time was also evaluated in another group of healthy subjects.

MATERIALS AND METHODS

Groups of Volunteers

The healthy volunteers included in this study were divided into 2 groups. In group 1, 6 young subjects (5 men, 1 woman; age, ~20 y; mean age, 19.5 ± 0.6 y) were included. All subjects underwent a 6-h scan. In group 2, 15 other subjects (6 men, 9 women; age, 20–71 y; mean age, 41.2 ± 18.7 y) were integrated. In this group, a short scan time was applied (90 min). None of the volunteers had a history of either neurologic or psychiatric illness or tobacco use. All subjects gave their written informed consent to participate in this study in compliance with the regulations of the Joint Committee on Clinical Investigation of the Kyoto University Hospital.

Radiolabeling

To a sodium ^{123}I-iodide solution (1,110 MBq) (Nihon Medi-Physics), 100 μg of 5-(tri-*n*-butylstannyl)-3-([1-*t*-butoxycarbonyl-2(*S*)-azetidinyl]methoxy)pyridine, 1.5% acetic acid, 3 mol L HCl, and 5% H_2O_2 solution were added, and the mixture was stirred at 75°C for 15 min. Concentrated HCl was then added and the resulting solution was stirred for another 10 min at 75°C. The mixture was made basic with sodium hydroxide and extracted with ethyl acetate, and the organic layer was evaporated. The residue was purified by reverse-phase high-performance liquid chromatography (HPLC) (Cosmosil 5C18-AR-300, 10 × 250 mm, Nacalai Tesque; 10 mmol L ammonium acetate:methanol:triethylamine = 752:750:2; 1.5 mL/min; retention time for 5IA = 40 min). After evaporation of the HPLC eluent, the residue was dissolved in 0.9% saline and filtered through a 0.2-μm filter into a sterile vial. Radiochemical purity was >98% and radiochemical yields were ~42%. The specific activity determined from the ultraviolet absorbance at 254 nm was >169 GBq μmol (the detection limit for this method).

SPECT

All SPECT dynamic scans were acquired with a triple-head rotating γ-camera system (PRISM 3000; Picker International, Inc.) equipped with low-energy, high resolution, fanbeam collimators. This system provides a spatial resolution of 8.0-mm full width at half maximum at the center of the field of view with a sensitivity of 135 cps/MBq. The volunteer's head was placed in a semicylindric head-holder lined with a rubber sponge to prevent motion during the study. Data acquisition was performed in 64 × 64 matrices in a continuous rotation mode with 40 steps for 120° and 1.5 s per step, which translate into 1 min for 1 SPECT dataset. For the first group of subjects, the 6-h scan time, volunteers underwent a 120-min scan (2 min × a 60-frames scan) after intravenous injection of ^{123}I-5IA, followed by 4 sets of 20-min scan (2 min × a 10-frames scan, at 3, 4, 5, and 6 h after the injection), while for the other group of volunteers, only a 90-min (2 min × a 45-frames scan) was performed in each subject.

A cross-calibration between the SPECT scanner and well counter was performed using a series of uniform cylindric phantoms (16-cm inner diameter × 15-cm height) containing an aqueous solution of ^{123}I. The activity on the SPECT images was linearly related to the activity concentration in the phantom measured with the automatic well-type γ-counter (Cobra 2; Packard).

All SPECT images were filtered with a Butterworth filter (cutoff frequency, 0.25; order, 4), and reconstructed using a filtered back-projection algorithm with a ramp filter. Attenuation correction was performed using ellipses outer line approximation and Chang's method (coefficient of 0.06 cm) adjusted for each slice, which assumes that the attenuation process is homogeneous throughout the brain and can be described by an exponential function. The same ellipse size was kept for the different scans of each volunteer. Scatter correction was not applied.

Arterial Input Function

A catheter was inserted into the left brachial artery for blood sampling, while another catheter was inserted into the right cubital vein for the injection of the radioligand. A dose of ~150 MBq ^{123}I-5IA was administered intravenously over a period of 1 min at a constant rate with an infusion pump. The scan started simultaneously with the injection.

An arterial input function was obtained for each volunteer. Twenty-five arterial blood samples were drawn, initially every 10 s during the first 2 min, followed by 15 s during the next minute, and then subsequently at 5, 7, 10, 20, 30, 45, 60, 90, and 120 min (for those subjects with a short scan time, the last sample was not drawn). Additionally, 6 venous blood samples were obtained at 1.5, 2, 3, 4, 5, and 6 h after injection using different vessels. Blood samples were centrifuged at 1,750*g* for 3 min at 4°C. From each sample, 100 μL of plasma were removed and the radioactivity was measured in an automatic well-type γ-counter (Cobra 2; Packard). All radioactivity measurements were decay corrected to the time of radioligand administration. The first 2 venous samples were drawn to verify the suitability of venous blood sampling to be used for the input function instead of arterial sampling. We previously confirmed its suitability in preliminary analytic studies of arterial and venous samples at several time points, including 1.5, 2, 4, and 6 h after injection.

Sixteen samples (1, 2, 3, 5, 7, 10, 20, 30, 45, 60, 90, 120, 180, 240, 300, and 360 min) were analyzed for metabolite determination. An aliquot of 300 μL of plasma was mixed with an equal volume of acetonitrile, and the denatured proteins were removed from the plasma by centrifugation at 1,750*g* for 5 min at 4°C. The radioactivity in the supernatant was analyzed by thin-layer chromatography (TLC) (R_f = 0.55 for ^{123}I-5IA) (LK6DF Silica Gel 60 Å; Whatman). The TLC plates were developed in a solution of 10% ammonium acetate and methanol (1:1). Furthermore, some of the plasma supernatant samples (1, 3, 10, 30, 60, and 120 min) were also analyzed by reverse-phase HPLC (Cosmosil 5C18-AR-300, 4.6 × 150 mm; Nacalai Tesque) at a flow rate of 1.0 mL/min (retention time for ^{123}I-5IA = 10 min).

The unmetabolized fraction, M(t), of the arterial input function was determined from the ratio of parent compound counts to the total plasma counts derived from TLC results. The following empiric equation was used to describe α and β:

$$M(t):1\ [1 + (\alpha t)^2]^{\beta}, \qquad \text{Eq. 1}$$

where the parameters α and β were estimated by nonlinear least-squares fitting. This empiric equation was designed to equal 1 at time 0 with a zero first derivative. Metabolite correction was performed by plotting the activity in arterial plasma samples against the time.

Data Analysis

Initially, 60 circular regions of interest (ROIs) (21 pixels per circle) were manually drawn on a 120-min composite transaxial SPECT image of each subject. The ROIs were distributed among various regions (basal ganglia, thalamus, brain stem, cerebellum, and frontal, parietal, temporal, and occipital cortices) on both sides. Then, ROIs were placed on the delayed scans (3-, 4-, 5-, and

6-h scans). To accomplish the best coregistration between the initial scan (120 min) and subsequent delayed scans (4 sets of 20 min), the slice with the highest tissue count (thalamus region) was identified for each scan. Then, based on that slice, the exact position of the ROIs used on the 120-min scan were repositioned on the other scans using an image analysis package (Dr. View; Asahi-Kasei) and dedicated software. Thus, we could maintain the same ROI position for the same region in different image sets. For the 90-min scan time, the same procedure was used. However, no coregistration with another scan time was necessary. ROI data were further decay corrected. SPECT data were calibrated to the well counter used to measure the injected activity. Time–activity curves were generated for each ROI using the same image analysis package (Dr. View).

Derivation of Receptor Parameters

The analysis of ^{123}I-5IA distribution begins with the kinetic model depicted in Figure 1A. Owing to the limited statistical quality of SPECT data, we initially proposed a model that has only 2 tissue compartments. The model consists of 1 blood compartment, representing the arterial plasma concentration of unchanged tracer (C_p), a tissue compartment (C_{f+ns}) that encloses free ligand in tissue (C_f) plus ligand bound to nonspecific sites (C_{ns}), and another tissue compartment representing ligand bound to specific sites (C_s). In this model, the free and nonspecifically bound tissue compartments are assumed to equilibrate rapidly. The units of concentration (or radioactivities) for each compartment presented in this article are in kBq g.

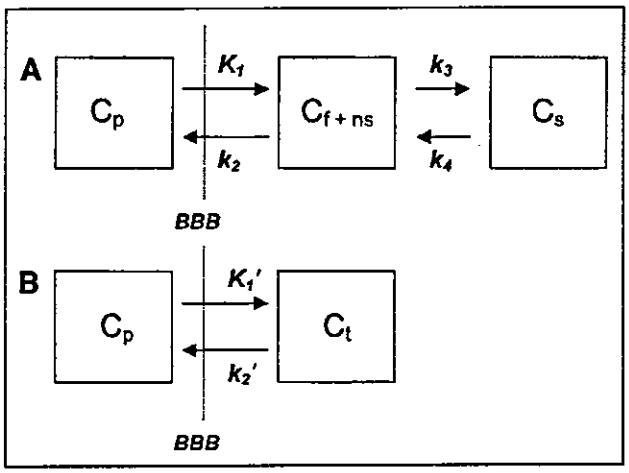

FIGURE 1. (A) Three-compartment, 4-parameter kinetic model. This model consists of 1 blood compartment (C_p), a tissue compartment (C_{f+ns}) that encloses the free ligand in tissue (C_f) plus ligand bound to nonspecific sites (C_{ns}), and another tissue compartment representing ligand bound to specific sites (C_s). Free and nonspecifically bound tissue compartments are assumed to equilibrate rapidly. Rate parameters (K_1, k_2, k_3, and k_4) describe exchange across blood–brain barrier (*BBB*), association and dissociation from sites in free plus nonspecifically bound compartment, and association and dissociation from sites in specifically bound compartment. (B) Two-compartment, 2-parameter kinetic model. This configuration simplifies the model described in A by combining free plus nonspecifically bound compartment and specific compartment into a single compartment (C_{f+ns+s}) and assumes that rate constants k_3 and k_4 are rapid compared with *BBB* transport rates.

The equilibrium distribution volume of a compartment i (V_i; mL g) was defined as the equilibrium ratio of the tracer concentration in this compartment (C_i) to the free arterial concentration ($C_p f_1$, where f_1 represents the fraction of unbound to plasma proteins unmetabolized parent radioligand activity in plasma):

$$V_i = C_i / C_p f_1. \quad \text{Eq. 2}$$

V_{f+ns} and V_s are the equilibrium distribution volumes of the free plus nonspecific compartments and specific compartment, respectively. V_{f+ns+s} (V_t) is the total regional equilibrium distribution volume, equal to the sum of V_{f+ns} and V_s.

The tracer concentration over time in C_{f+ns} and C_s is given by:

$$dC_{f+ns}(t)/dt = K_1 C_p(t) - k_2 C_{f+ns}(t) - k_3 C_{f+ns}(t) + k_4 C_s(t). \quad \text{Eq. 3}$$

$$dC_s(t)/dt = k_3 C_{f+ns}(t) - k_4 C_s(t). \quad \text{Eq. 4}$$

The parameters are defined as follows:

$$K_1 = FE_0 = f(1 - e^{-PS/F}) \text{ (mL g min)}. \quad \text{Eq. 5}$$

$$k_2 = K_1 / V_{f+ns} f_1 \text{ (min}^{-1}\text{)}. \quad \text{Eq. 6}$$

$$k_3 = k_{on} B_{max}' V_{f+ns} \text{ (min}^{-1}\text{)}. \quad \text{Eq. 7}$$

$$k_4 = k_{off} \text{ (min}^{-1}\text{)}. \quad \text{Eq. 8}$$

$$K_d = k_{off}/k_{on}. \quad \text{Eq. 9}$$

$$k_3/k_4 = B_{max}'/K_d = BP. \quad \text{Eq. 10}$$

The rate parameter K_1 represents the delivery rate constant from plasma to compartment C_{f+ns}, and k_2 defines the rate constant of return from compartment C_{f+ns} to plasma. We assume that, at equilibrium, the concentration of free tracer in tissue water equals the concentration in plasma water. The parameter k_3 is the rate constant of transfer from compartment C_{f+ns} to C_s, and the parameter k_4 is equal to k_{off}, the dissociation rate from the receptor.

The parameter F is regional blood flow (mL g min). E_0 is the single-pass extraction fraction of ligand into brain. PS is the permeability-surface area product (mL g min). k_{on} is the biomolecular association rate between ligand and receptor (g pmol min). B_{max}' is the receptor density or concentration of "unoccupied" receptors (pmol g). k_{off} is the dissociation rate of ligand from the receptor complex (min^{-1}), and K_d is the equilibrium ligand binding constant for the specific receptor site (pmol g). The ratio of receptor-related parameters B_{max}' and K_d has been previously referred to as the binding potential (BP) (25). The solution to this model form is given by:

$$C_t(t) = K_1 (x_2 - x_1)[(k_3 + k_4 - x_1)e^{-x_1 t} + (x_2 - k_3 - k_4)e^{-x_2 t}] \otimes C_p(t), \quad \text{Eq. 11}$$

where $C_t(t)$ is defined as concentration in tissue ($C_{f+ns} + C_s$):

$$x_{1,2} = \frac{(k_2 + k_3 + k_4) \pm \sqrt{(k_2 + k_3 + k_4)^2 - 4k_2k_4}}{2}. \quad \text{Eq. 12}$$

$\otimes$ represents the mathematic operation of convolution.

If the binding and dissociation of ligand from the specific receptor compartment are rapid compared with the transport parameters K_1 and k_2, the model can be further reduced to a single tissue compartment that contains free, nonspecifically bound, and specifically bound ligand, as shown in Figure 1B. The kinetic parameters of this simplified model are described as follows:

$$K_1' = FE_0 = f(1 - e^{-PS/F}). \quad \text{Eq. 13}$$

$$k_2' = k_2 (1 + k_3/k_4) = K_1 V_{f+ns}'/f_1 = K_1 V_{f+ns+s}/f_1. \quad \text{Eq. 14}$$

$$V_{f+ns}' = V_{f+ns+s} = K_1/k_2' = V_T. \quad \text{Eq. 15}$$

The solution equation to this model form is given by:

$$C_t(t) = K_1 \cdot e^{-k_2' t} \otimes C_p(t). \quad \text{Eq. 16}$$

Since k_3 and B_{max}' are no longer isolated model parameters, receptor information in this model configuration is represented only by V_T. As the ratio of the association to dissociation rate (k_3/k_4) becomes progressively higher, the specific distribution volume term dominates and V_{f+ns}' yields a progressively better estimate of B_{max}'.

Due to its simplicity and independence from a model—that is, no knowledge is required of the compartmental configuration of the underlying data—a graphical method of analysis (*26*) was also used. In SPECT, regions of brain tissue are sampled by drawing a ROI. The radioactivities in a ROI at time t can be expressed as:

$$ROI(t) = C_t(t) + VC_p(t), \quad \text{Eq. 17}$$

that is, the sum of radioactivities from all compartments in a given ROI plus the contribution from regional blood volume V. V is estimated at 5% and often has a negligible contribution after the initial part of the study. Thus, Equation 17 can be rearranged into Equations 18 and 19 for the 3- and 2-compartmental models, respectively:

$$\int_0^t \mathrm{ROI}(t')dt' \,\mathrm{ROI}(t) =$$

$$[K_1/k_2(1 + k_3/k_4) + V] \int_0^t C_p(t')dt' \,\mathrm{ROI}(t) + int. \quad \text{Eq. 18}$$

$$\int_0^t \mathrm{ROI}(t')dt' \,\mathrm{ROI}(t) = (K_1/k_2' + V) \int_0^t C_p(t')dt' \,\mathrm{ROI}(t) + int.$$

Eq. 19

Equations 18 and 19 are linear forms when the last term (*int*) is constant. The points plotted are defined by the scanning time t.

Plotting $\int_0^t \mathrm{ROI}(t')dt' \,\mathrm{ROI}(t)$ versus $\int_0^t C_p(t')dt' \,\mathrm{ROI}(t)$ for time t, a representative plot of a ROI is linear after some time t^*. The slope of this linear function represents the total distribution volume plus the blood contribution, here defined as V_{LG}. In this study, the K_1 value from the Logan plot is designated as K^*_1 as well as k^*_2. The effects of blood flow and capillary permeability are implicitly included in K^*_1 and k^*_2. For the 2-compartment model, nonspecific binding is also included in k^*_2. Estimates of K^*_1 can be calculated by taking the ratio of the slope (V_{LG} value, neglecting V) of the linear function, while k^*_2 can be calculated by taking the ratio of K^*_1 to V_{LG}. This will be valid for the 2-compartment model when the second term, the intercept, is small compared with the first.

Statistical Analysis

All data are expressed as the mean ± SD and the percentage of the rate constants (coefficient of variation [%COV]) (100 × SD/mean). The distribution volumes obtained from the different regions in the brain were analyzed using 1-way ANOVA with the Bonferroni protected least-significant difference test. A factorial ANOVA was also performed considering interacted factors, different time intervals (90 and 360 min) and regions in the brain, to determine the V_T values. An analysis of correlation (Pearson test) between distribution volumes calculated from different methods of analyses was performed. A Student t test was also applied for comparisons between the first (90-min scan time) and second group of volunteers with matched age for the same region. All tests were 2-sided, and P values <0.05 were considered significant.

RESULTS

Plasma Analysis

For group 1 volunteers and the 6-h scan time, the peak plasma activity occurred between 70 and 80 s after injection in all subjects and decreased rapidly to 3.6%–7.9% of the peak level in 10 min. Analysis of the unmetabolized compound by TLC demonstrated a high parent fraction of ^{123}I-5IA in the plasma (89.9% ± 5.1%) in the first minute. These values were estimated using Equation 1, which showed good fitting for all volunteers. ^{123}I-5IA was rapidly metabolized and the unchanged fraction represented 46.6% ± 9.5% and 27.4% ± 6.0% of total plasma activity at 20 and 60 min, respectively. Figure 2 shows typical radioactivity in whole plasma and the free parent compound of ^{123}I-5IA throughout the scan time. For the 90-min scan time, the second group of volunteers, the results were similar to those described for the 6-h scan time.

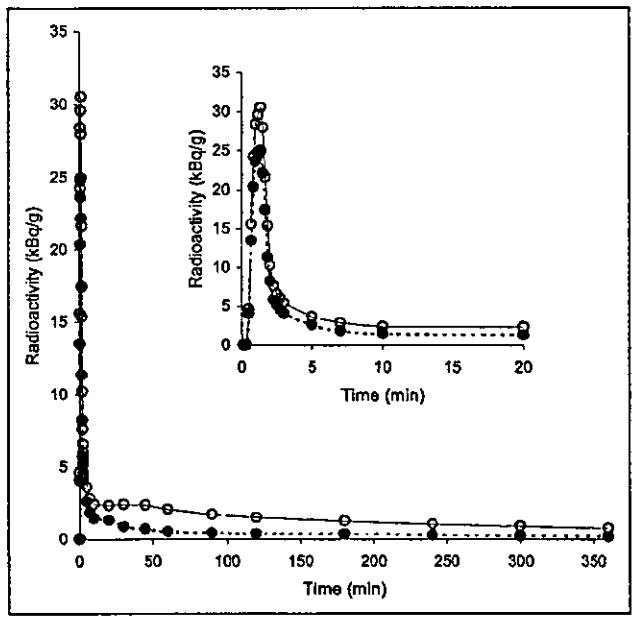

FIGURE 2. Typical plasma time–activity curves show radioactivity in whole plasma (○) and free parent (●) compound of ^{123}I-5IA acquired throughout scan time (360 min) after intravenous bolus injection of 172 MBq ^{123}I-5IA in 20-y-old man (subject 4). Inset shows same plasma time–activity curves for short period (20 min). Peak plasma activity occurred at 80 s after injection of ^{123}I-5IA and decreased rapidly to 5.9% of peak level in 10 min.

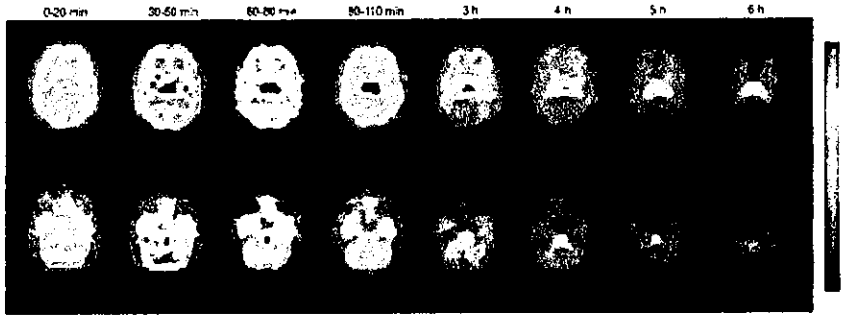

FIGURE 3. Selected slices of human brain after intravenous bolus injection of 172 MBq ^{123}I-5IA in 20-y-old man (subject 4). Reconstructed tranverse slices were summed according to scan time (0–20 min, 30–50 min, 60–80 min, 90–110 min, 3 h, 4 h, 5 h, and 6 h). Top row of slices represents midpart of brain (frontal, temporal, occipital, thalamus, and basal ganglia). Bottom row represents slices from inferior part of human brain (cerebellum, brain stem, and temporal cortex). ^{123}I-5IA SPECT images clearly show cortical regions, cerebellum, thalamus, brain stem, and basal ganglia. Thalamus and brain stem exhibited higher uptake than other structures in brain, which became more prominent throughout scan time.

The suitability of using venous blood sampling for the input function was confirmed by the good agreement of the radioactivity in whole plasma (0.00099 ± 0.00015 [arterial] and 0.00100 ± 0.00013 [venous] %dose/mL at 90 min; 0.00090 ± 0.00011 [arterial] and 0.00094 ± 0.00012 [venous] %dose/mL at 120 min) and the ratio of measured free parent fraction between arterial and venous blood samples drawn at 90 and 120 min (0.29 ± 0.05 [arterial] and 0.27 ± 0.04 [venous] at 90 min; 0.20 ± 0.04 [arterial] and 0.20 ± 0.04 [venous] at 120 min). Thus, venous blood sampling is a simple and acceptable choice for input function following 2 h after injection of 5IA.

The results obtained by TLC were in agreement with those from HPLC at 1, 3, 10, 30, 60, and 120 min after injection. The labeled metabolites were not identified, but they were more polar than the parent compound and may not cross the blood–brain barrier.

Brain Imaging Analysis

For all volunteers (first and second groups), ^{123}I-5IA-SPECT images clearly revealed the cortical regions, cerebellum, thalamus, brain stem, and basal ganglia. Initially, within the first 20 min, the images seemed to have a similar pattern as cerebral blood flow. Subsequently, the thalamus and brain stem showed higher uptake than the other structures in the brain, which became more prominent throughout the scan time. Figure 3 shows a typical 6-h scan time distribution and the dynamics of ^{123}I-5IA in the brain throughout the scan time. No side effects were observed during the scan in any volunteers.

Figure 4 shows typical 6-h scan time–activity curves of ^{123}I-5IA in the thalamus, brain stem, and frontal cortex. The concentration of radioactivity was highest in the thalamus followed by the brain stem. An intermediate accumulation of radioactivity of ^{123}I-5IA was observed in the cerebellum, basal ganglia, and cortical regions. In all subscripts, the peaks of radioactivity in the thalamus and brain stem occurred at 90–110 min and 70–90 min after injection of ^{123}I-5IA, respectively. These peaks were observed later than in the other brain regions, which were found at around 30–50 min. A differential dissociation of ^{123}I-5IA from the binding sites was noted in the brain. The cortical regions, basal ganglia, and cerebellum showed an earlier dissociation than the brain stem and thalamus. These findings reflected a distinct regional distribution of nAChRs in the human brain (*27,28*).

For the second group of volunteers, the pattern of radioactivity in the brain was almost the same as that described for the first group, except for the thalamus. The peak of radioactivity in the thalamus could not be seen precisely throughout the scan time. The time–activity curve in the cortical regions, basal ganglia, and cerebellum had a similar pattern observed during the 6-h scan time.

Based on these data, a quantitative analysis of nAChR density was performed. First, the 3-compartment model analysis was performed. The 4-parameter model configura-

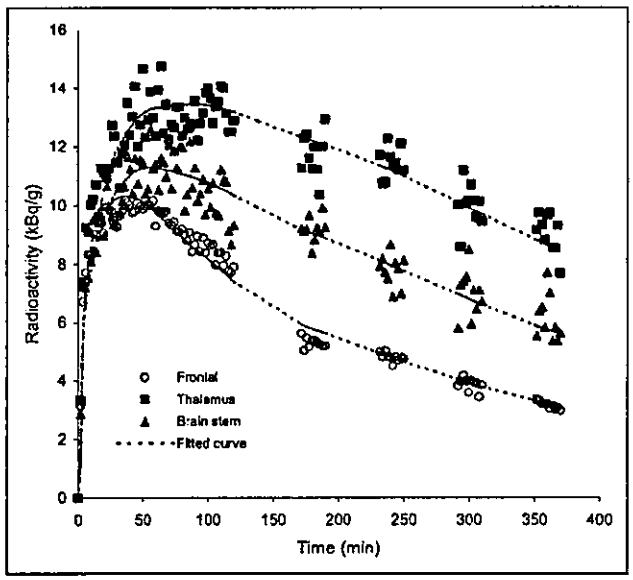

FIGURE 4. Typical time–activity curves of ^{123}I-5IA in regions of human brain after intravenous injection of 172 MBq ^{123}I-5IA in 20-y-old man (subject 4). Concentration of radioactivity in brain was highest in thalamus followed by brain stem. Little accumulation of radioactivity was observed in cortical regions (represented by frontal cortex).

TABLE 1

^{123}I-5IA Parameter Estimates for 2-Compartment, 2-Parameter Model Analysis Using 6-Hour Scan Time (6 Healthy Volunteers)

	Frontal cortex			Parietal cortex			Temporal cortex			Occipital cortex			Basal ganglia			Thalamus			Brain stem			Cerebellum		
Volunteer	V_T	K_1'	k_2'	V_T	K_1'	k_2'	V_T	K_1'	k_2'	V_T	K_1'	k_2'	V_T	K_1'	k_2'	V_T	K_1'	k_2'	V_T	K_1'	k_2'	V_T	K_1'	k_2'
1																								
Mean	19.0	0.21	0.011	17.8	0.22	0.012	18.5	0.20	0.011	17.5	0.20	0.012	23.1	0.20	0.009	47.1	0.22	0.005	35.2	0.21	0.006	19.9	0.23	0.012
SD	0.2	0.01	0.001	0.2	0.01	0.000	0.7	0.01	0.001	0.7	0.01	0.001	0.4	0.02	0.001	1.8	0.01	0.000	1.2	0.01	0.000	0.9	0.02	0.001
%COV	1.1	6.0	5.4	1.1	2.8	3.5	3.5	5.4	6.6	4.1	3.7	6.6	1.7	7.9	8.7	3.7	3.2	5.3	3.5	6.6	4.9	4.6	6.7	9.1
2																								
Mean	13.6	0.21	0.016	13.4	0.22	0.016	13.1	0.20	0.016	12.0	0.21	0.018	15.3	0.21	0.014	31.3	0.19	0.006	22.6	0.19	0.009	17.0	0.19	0.011
SD	0.3	0.01	0.000	0.4	0.01	0.001	0.6	0.01	0.001	0.5	0.01	0.001	0.7	0.01	0.001	1.9	0.01	0.000	0.9	0.00	0.000	0.1	0.01	0.000
%COV	2.0	2.4	2.1	3.1	3.5	6.2	4.9	5.5	6.7	3.8	5.1	6.4	4.4	5.2	5.9	6.2	2.9	5.7	3.8	1.3	4.4	0.9	3.4	3.6
3																								
Mean	16.2	0.27	0.017	16.3	0.26	0.016	16.6	0.26	0.016	15.2	0.27	0.018	21.3	0.23	0.011	37.1	0.23	0.006	26.3	0.24	0.009	20.1	0.28	0.014
SD	0.3	0.01	0.001	0.5	0.02	0.001	0.3	0.01	0.001	0.5	0.01	0.001	0.6	0.00	0.000	1.8	0.02	0.001	1.3	0.01	0.001	0.5	0.01	0.001
%COV	2.2	3.6	4.1	2.8	6.9	7.0	1.6	3.9	4.3	3.6	4.8	6.5	2.7	1.2	3.1	4.7	7.2	9.5	5.0	3.6	8.4	2.4	4.9	5.0
4																								
Mean	12.9	0.19	0.015	12.6	0.18	0.015	12.7	0.18	0.014	11.6	0.20	0.017	15.0	0.17	0.011	29.1	0.18	0.006	20.0	0.17	0.009	15.8	0.19	0.012
SD	0.6	0.01	0.001	0.3	0.00	0.000	0.5	0.01	0.001	0.3	0.01	0.001	0.4	0.02	0.002	1.8	0.01	0.001	1.3	0.01	0.001	0.5	0.01	0.000
%COV	4.3	6.2	5.2	2.1	2.0	3.4	3.9	6.5	4.4	2.9	3.7	4.4	2.4	13.2	15.2	6.1	6.8	9.0	6.6	6.8	8.9	3.0	4.0	3.4
5																								
Mean	13.0	0.24	0.019	11.9	0.23	0.019	12.6	0.23	0.018	11.3	0.25	0.023	14.4	0.23	0.016	29.0	0.23	0.008	20.0	0.21	0.010	15.6	0.23	0.015
SD	0.5	0.01	0.001	0.5	0.02	0.002	0.2	0.01	0.001	0.4	0.01	0.001	0.4	0.01	0.001	1.5	0.01	0.000	1.1	0.01	0.001	0.7	0.01	0.001
%COV	4.1	5.7	3.6	4.5	7.9	8.5	1.7	4.8	3.5	3.4	3.2	5.1	3.0	3.3	5.1	5.1	3.4	4.6	5.4	4.0	8.1	4.3	2.7	4.2
6																								
Mean	13.1	0.18	0.014	13.3	0.19	0.014	13.9	0.17	0.012	11.6	0.18	0.016	16.3	0.17	0.010	32.4	0.18	0.006	24.2	0.17	0.007	18.4	0.21	0.012
SD	0.6	0.01	0.001	0.6	0.01	0.001	0.1	0.01	0.000	0.1	0.01	0.001	0.1	0.01	0.001	1.2	0.01	0.001	0.8	0.00	0.000	0.9	0.01	0.001
%COV	4.4	6.8	4.0	4.5	4.9	8.3	1.1	3.1	2.6	1.2	5.3	4.9	0.8	5.0	5.3	3.7	8.1	9.3	3.3	2.3	1.8	4.9	6.0	9.1
All																								
Mean	14.6	0.22	0.015	14.2	0.21	0.015	14.6	0.21	0.014	13.2	0.22	0.017	17.6	0.20	0.012	34.3	0.21	0.006	24.7	0.20	0.008	17.8	0.22	0.013
SD	2.5	0.03	0.003	2.3	0.03	0.002	2.4	0.03	0.003	2.6	0.03	0.004	3.7	0.03	0.003	6.9	0.03	0.001	5.7	0.02	0.002	2.0	0.03	0.001
%COV	16.8	15.1	16.8	16.3	12.5	14.8	16.7	16.8	18.8	19.4	15.0	20.6	20.9	13.3	21.2	20.2	12.5	17.4	22.9	12.3	18.7	11.0	14.0	11.8

Values for V_T are given in mL/g, for K_1' in mL/g/min, and for k_2' in min^{-1}.

tion could not appropriately fit the present data and inadequately identified the rate parameter constants. Variable lower V_T values in different regions in the human brain were also observed (data not shown). The 3-compartment model could not provide goodness of fit, indicating that the association and dissociation of ligand from the specific receptor compartment were rapid, and the nonspecific and specific compartments mixed instantaneously. Thus, all analyses were made with the 2-compartment model.

Table 1 summarizes the V_T, K_1', and k_2' values from 2-compartment model analysis in different brain regions for each subject studied in the first group. The highest V_T values were found in the thalamus (ANOVA, $P < 0.01$). Subsequently, the brain stem, cerebellum, and basal ganglia were assembled in a group of moderate $\alpha_4\beta_2$ binding density. No statistically significant difference was observed between them. The V_T values of the brain stem and cerebellum were higher ($P < 0.05$) than the values for the cortical regions (frontal, parietal, temporal, and occipital cortices), whereas for the basal ganglia this finding was observed only for the occipital cortex ($P < 0.05$). The remaining regions were arranged in a group of low-binding density. The relative performance of the 2-parameter model configuration can be evaluated through comparison of the estimated parameters using %COV. The estimation of parameters V_T, K_1', and k_2' is relatively stable and the variation was small in each subject across all brain regions (Table 1). The intersubject variability was also reasonable and generally ranged from 11% to 21%.

Figure 5 illustrates a typical example of graphical analysis applied to ROIs from the frontal cortex, thalamus, and brain stem. The linear region begins at about 4 min after injection (t^*). The same time point (t^*) was observed for all subjects across all regions. The slope is greatest for the ROI from the thalamus, followed by the brain stem and frontal cortex. Table 2 lists V_{LG}, K^*_1, and k^*_2 determined by the graphical analysis in the brain. The pattern of distribution of V_{LG} in the human brain was the same as that of V_T in all subjects at the 6-h scan time, as was the variability accounted for by %COV.

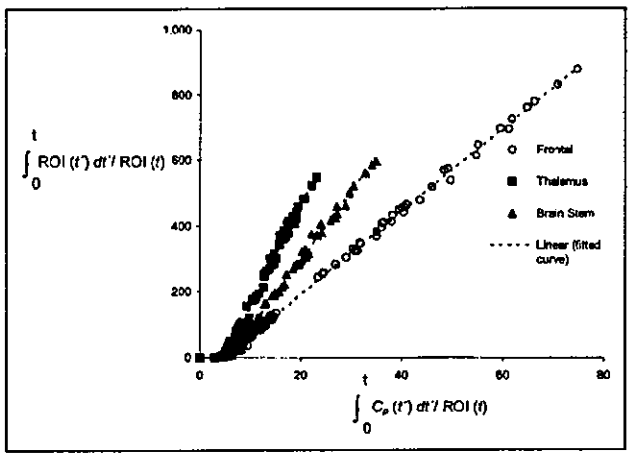

FIGURE 5. Typical example of graphical analysis applied to ROIs from frontal cortex, thalamus, and brain stem (subject 4). At about 4 min after injection (t^*), a representative plot of ROI is linear. Slope of this linear function represents total distribution volume plus blood contribution (V_{LG}). Greatest slope is for ROI from thalamus, followed by brain stem and frontal cortex. Slopes representative of linear curves are 10.5, 15.7, and 13.3, respectively.

Parameter estimates as a function of the duration of data used in the fits from the 6-h scan time are shown in Table 3. Estimations were made using a short time interval (0–90 min) for the entire 360-min sequence. The estimation of parameters V_T, K_1', and k_2' is quite stable in the cortical regions and basal ganglia throughout the time intervals. On the other hand, some variability was observed in the thalamus, brain stem, and cerebellum for a shorter scan time. One-way ANOVA demonstrated no significant difference between those time intervals across all regions.

Table 4 summarizes the receptor parameter values (V_T, K_1', and k_2') from the 2-compartment model analysis in different brain regions for each volunteer in a short scan time (90 min). Results of the first 6 volunteers (subjects 1–6, group 1) were generated from a 6-h scan time when a short time interval (0–90 min) was applied. Results of the remaining 15 volunteers (subjects 7–21, group 2) were calculated from a single 90-min scan time. To verify the homogeneity of V_T values determined between these 2 groups of subjects, aged-matching comparisons were done. The V_T values from the first group of subjects were compared with those from the second group with the same age. No statistical differences were observed between V_T values for all regions in the brain between these 2 groups of subjects for the same age. The distribution of V_T values for all subjects with a short scan time (first and second groups) had a pattern similar to that observed for a 6-h scan time. The thalamus showed also the highest V_T value (ANOVA, $P < 0.01$).

DISCUSSION

To our knowledge, this article describes the first quantitative study of ^{123}I-5IA SPECT for the measurement of nAChRs in the human brain. There were several reasons for selecting ^{123}I-5IA to quantitatively study nAChRs in the human brain. First, there were several previous studies of radioiodine-labeled compounds of these series with extremely high affinity and selectivity for the nAChR $\alpha_4\beta_2$ subtype in vivo, with low nonspecific binding, good persistence in animal and human brain, and acceptable dosimetry for human use (*19–24*). Second, the procedure for the synthesis of ^{123}I-5IA is not complicated, the radiochemical purity is high (>98%), the radiochemical yields are good (42%), and highly specific radioactivity can be achieved with this radiolabeling sequence (*18*). Third, the longer imaging time frame afforded with ^{123}I (half-life = 13.2 h) and the prevalence of SPECT scanners in laboratories

TABLE 2

^{123}I-5IA Parameter Estimates for Graphical Analysis from 2-Compartment Model Using 6-Hour Scan Time (6 Healthy Volunteers)

	Frontal cortex			Parietal cortex			Temporal cortex			Occipital cortex			Basal ganglia			Thalamus			Brain stem			Cerebellum		
Volunteer	V_{LG}	K^*_1	k^*_2	V_{LG}	K^*_1	k^*_2	V_{LG}	K^*_1	k^*_2	V_{LG}	K^*_1	k^*_2	V_{LG}	K^*_1	k^*_2	V_{LG}	K^*_1	k^*_2	V_{LG}	K^*_1	k^*_2	V_{LG}	K^*_1	k^*_2
1																								
Mean	18.4	0.22	0.012	17.6	0.23	0.013	18.2	0.20	0.011	17.9	0.20	0.011	23.1	0.20	0.009	45.6	0.23	0.005	34.8	0.21	0.006	20.3	0.23	0.012
SD	0.4	0.02	0.001	0.5	0.01	0.001	1.1	0.01	0.001	0.4	0.00	0.000	0.4	0.02	0.001	1.4	0.01	0.000	1.5	0.01	0.000	0.9	0.02	0.002
%COV	2.0	7.0	6.5	2.7	5.0	7.5	6.2	6.9	10.7	2.5	2.0	3.4	1.6	8.3	9.1	3.0	3.1	5.4	4.3	6.0	2.7	4.3	9.5	13.2
2																								
Mean	13.2	0.23	0.017	13.1	0.22	0.017	13.0	0.21	0.016	12.0	0.22	0.018	15.5	0.21	0.014	31.6	0.19	0.006	23.0	0.19	0.008	17.2	0.19	0.011
SD	0.4	0.01	0.001	0.5	0.01	0.002	0.8	0.01	0.001	0.5	0.02	0.002	1.0	0.01	0.001	1.1	0.01	0.000	1.1	0.00	0.000	0.3	0.01	0.001
%COV	3.2	5.5	6.9	4.0	6.1	10.1	5.9	5.5	6.5	4.5	7.8	10.9	6.5	5.4	9.6	3.3	3.5	3.8	4.7	1.0	5.1	1.9	4.0	5.6
3																								
Mean	16.1	0.27	0.017	16.6	0.27	0.016	16.9	.026	0.016	15.5	0.28	0.018	21.9	0.23	0.011	37.3	0.24	0.006	26.8	0.24	0.009	20.9	0.27	0.013
SD	0.5	0.02	0.002	0.6	0.03	0.002	0.6	0.01	0.001	0.6	0.02	0.001	1.1	0.01	0.001	1.4	0.01	0.000	1.2	0.01	0.001	0.5	0.02	0.001
%COV	3.2	7.5	9.6	3.6	10.1	11.3	3.5	4.3	6.9	4.0	6.2	7.1	4.8	2.4	7.1	3.7	5.7	6.1	4.6	4.0	8.5	2.2	5.6	6.5
4																								
Mean	12.6	0.20	0.016	12.2	0.20	0.017	12.4	0.19	0.015	11.2	0.23	0.021	14.9	0.17	0.012	28.9	0.19	0.007	19.5	0.18	0.009	16.1	0.20	0.012
SD	0.3	0.02	0.001	0.04	0.01	0.001	0.4	0.02	0.001	0.4	0.02	0.003	0.5	0.02	0.002	2.0	0.01	0.001	1.1	0.01	0.001	0.4	0.01	0.001
%COV	2.5	9.4	9.2	3.2	4.0	6.2	3.3	8.9	8.8	3.6	9.5	12.3	3.3	12.8	15.2	7.0	3.8	9.0	5.5	7.2	7.6	2.7	5.0	5.1
5																								
Mean	12.9	0.27	0.021	11.8	0.24	0.021	12.6	0.24	0.019	11.4	0.26	0.023	15.2	0.22	0.014	29.0	0.24	0.008	20.3	0.22	0.011	16.1	0.23	0.015
SD	0.3	0.02	0.002	0.4	0.02	0.001	0.3	0.01	0.001	0.5	0.02	0.003	0.5	0.01	0.001	1.0	0.01	0.000	0.9	0.01	0.001	0.6	0.01	0.001
%COV	2.4	7.3	7.3	3.5	6.2	5.8	2.3	5.7	4.5	4.2	7.9	11.4	3.1	3.4	5.7	3.3	3.0	5.6	4.4	3.3	6.3	3.7	3.4	3.8
6																								
Mean	12.5	0.21	0.017	13.0	0.21	0.016	13.3	0.19	0.014	11.7	0.20	0.017	16.0	0.18	0.011	31.5	0.19	0.006	22.3	0.19	0.008	18.2	0.22	0.012
SD	0.5	0.01	0.001	0.4	0.02	0.002	0.2	0.01	0.001	0.3	0.02	0.002	0.4	0.01	0.001	1.5	0.01	0.000	0.6	0.01	0.000	0.8	0.01	0.001
%COV	4.0	7.1	5.3	2.7	8.7	9.7	1.2	5.4	6.1	2.4	8.8	10.4	2.7	5.8	7.3	4.8	5.4	3.6	2.8	3.0	1.9	4.5	5.6	8.6
All																								
Mean	14.3	0.23	0.017	14.0	0.23	0.017	14.4	0.22	0.015	13.3	0.23	0.018	17.8	0.20	0.012	34.0	0.21	0.006	24.5	0.20	0.009	18.1	0.23	0.013
SD	2.4	0.03	0.003	2.4	0.02	0.002	2.5	0.03	0.003	2.8	0.03	0.004	3.7	0.02	0.002	6.4	0.03	0.001	5.7	0.02	0.001	2.1	0.03	0.001
%COV	16.9	13.2	16.5	17.4	10.5	14.9	17.4	13.7	17.0	20.8	14.7	22.1	20.9	11.4	17.9	19.0	12.1	17.2	23.2	11.3	17.1	11.4	12.2	9.3

Values for V_{LG} are given in mL/g, for K^*_1 in mL/g/min, and for k^*_2 in min^{-1}.

TABLE 3

^{123}I-5IA Parameter Estimates For 2-Compartment, 2-Parameter Model Analysis with 6-Hour Scan Time at Different Time Intervals

Volunteer	Frontal cortex			Parietal cortex			Temporal cortex			Occipital cortex			Basal ganglia			Thalamus			Brain stem			Cerebellum		
	V_T	K_1'	k_2'	V_T	K_1'	k_2'	V_T	K_1'	k_2'	V_T	K_1'	k_2'	V_T	K_1'	k_2'	V_T	K_1'	k_2'	V_T	K_1'	k_2'	V_T	K_1'	k_2'
360 min																								
Mean	14.6	0.22	0.015	14.2	0.21	0.015	14.6	0.21	0.014	13.2	0.22	0.017	17.6	0.20	0.012	34.3	0.21	0.006	24.7	0.20	0.008	17.8	0.22	0.013
SD	2.5	0.03	0.003	2.3	0.03	0.002	2.4	0.03	0.003	2.6	0.03	0.004	3.7	0.03	0.003	6.9	0.03	0.001	5.7	0.02	0.002	2.0	0.03	0.001
%COV	16.8	15.1	16.8	16.3	12.5	14.8	16.7	16.8	18.8	19.4	15.0	20.6	20.9	13.3	21.2	20.2	12.5	17.4	22.9	12.3	18.7	11.0	14.0	11.8
90 min																								
Mean	14.8	0.21	0.015	14.1	0.22	0.016	14.1	0.21	0.015	12.6	0.23	0.018	16.2	0.22	0.014	28.4	0.23	0.009	21.8	0.21	0.010	16.1	0.24	0.015
SD	2.1	0.03	0.002	2.5	0.03	0.003	1.9	0.04	0.003	2.1	0.03	0.004	3.8	0.04	0.004	7.2	0.04	0.003	4.8	0.03	0.003	2.1	0.04	0.003
%COV	14.3	15.8	15.5	17.7	14.3	19.9	13.6	18.0	16.9	16.7	15.2	19.6	23.8	17.1	25.1	25.2	17.6	29.8	22.1	15.4	30.0	12.7	16.2	19.1

Values for V_T are given in mL/g, for K_1' in mL/g/min, and for k_2' in min^{-1}.

worldwide, with no requirement for an on-site cyclotron for positron-emitters, might provide some advantages, although the spatial resolution of SPECT systems is lower, and the quantitative accuracy of the SPECT data is poor compared with that of dedicated PET systems. Fourth, the satisfactory safety profile of this compound, with such a high specific activity, ensures that the administration dose of ^{123}I-5IA is well below the threshold at which pharmacologic effects first appear (*18–21,23,24*).

The quantitative analysis of ^{123}I-5IA was performed using a compartmental model. First, the 3-compartment model was chosen. This configuration might theoretically be a better choice for estimating the kinetic parameters for ^{123}I-5IA; however, the 4-parameter configuration could not provide goodness of fit for the present data—namely, it seemed that the ^{123}I-5IA in nonspecific and specific compartments mixed immediately. Therefore, 4-parameter kinetic analysis seemed to be an unsuitable choice for quantification of human nAChRs using ^{123}I-5IA SPECT. Thus, the quantitative V_T values in various regions of the human brain were estimated by 2-compartment model analysis. The 2-compartment model has a small number of parameters to be identified in the brain, making this choice simpler and acceptable for ^{123}I-5IA. This fact could be observed by the relatively stable performance of the estimated parameters using %COV (Table 1).

The V_T values from 2-compartment model analyses using the 6-h scan time showed the highest density of nAChRs in the thalamus; moderate density in the brain stem, basal ganglia, and cerebellum; and low density in the frontal, parietal, temporal, and occipital cortices. This distribution is compatible with the known distribution of nicotinic receptors in humans (*2*). A previous autoradiographic study using ^{3}H-epibatidine, which has similar affinity for the $\alpha_4\beta_2$ subtype of nAChR, described 3 levels of density of nAChRs in the human brain (high, moderate, and low) (*29*). The results of the present study are consistent with those for almost all regions evaluated in the study of Marutle et al. (*29*). Shimohama et al. (*10*) described the regional distribution of nAChRs in human brain using (−)-^{3}H-nicotine in an in vitro receptor assay study. The distribution volumes described for ^{123}I-5IA at 360 min after injection correlated well with the nAChR densities measured using (−)-^{3}H-nicotine (r^2 = 0.91) (Fig. 6), although there is some variation at the area with low density of nAChRs. Some divergence in the affinity of these compounds to the nAChR $\alpha_4\beta_2$ subtype, associated with some affinity toward other subunits in the brain, could explain these small differences (*15,29,30*). Thus, the possibility that ^{123}I-5IA binds with other mammalian nAChR subtypes cannot be excluded (*17,29,31*). In addition, significant losses or upregulation of nAChRs in the brain have been related to various situations, such as normal aging, neurodegenerative diseases, and tobacco use (*2,7–10,29*). In this context, ^{123}I-5IA will provide valuable information from living subjects in various clinical situations.

TABLE 4

^{123}I-5IA Parameter Estimates for 2-Compartment, 2-Parameter Model Analysis with 90-Minute Scan Time

Volunteer			Frontal cortex			Parietal cortex			Temporal cortex			Occipital cortex			Basal ganglia			Thalamus			Brain stem			Cerebellum		
No.	Sex	Age (y)	V_T	K_1'	k_2'	V_T	K_1'	k_2'	V_T	K_1'	k_2'	V_T	K_1'	k_2'	V_T	K_1'	k_2'	V_T	K_1'	k_2'	V_T	K_1'	k_2'	V_T	K_1'	k_2'
1	M	20	13.3	0.18	0.013	12.7	0.19	0.015	13.1	0.17	0.013	10.8	0.20	0.018	14.7	0.18	0.012	30.4	0.18	0.006	20.8	0.18	0.009	17.3	0.22	0.013
2	F	20	13.2	0.24	0.018	11.3	0.24	0.021	12.3	0.23	0.019	10.7	0.27	0.025	12.8	0.25	0.020	23.3	0.26	0.011	15.4	0.25	0.016	13.4	0.27	0.020
3	M	20	13.4	0.18	0.014	12.9	0.18	0.014	12.9	0.18	0.014	11.8	0.20	0.017	13.9	0.18	0.013	23.3	0.20	0.009	20.0	0.17	0.009	14.2	0.21	0.015
4	M	20	16.3	0.27	0.017	15.8	0.27	0.017	16.0	0.28	0.017	14.9	0.27	0.019	18.1	0.27	0.015	24.6	0.29	0.012	24.2	0.25	0.011	18.2	0.31	0.017
5	M	20	14.2	0.21	0.015	13.9	0.21	0.015	13.2	0.20	0.015	11.9	0.21	0.018	14.4	0.22	0.015	26.4	0.20	0.008	20.7	0.20	0.010	15.7	0.21	0.013
6	M	20	18.4	0.22	0.012	18.2	0.22	0.012	17.0	0.21	0.012	15.6	0.22	0.014	22.1	0.22	0.010	41.7	0.23	0.006	29.9	0.22	0.008	18.1	0.24	0.014
7	F	20	17.8	0.24	0.014	16.5	0.24	0.014	17.4	0.25	0.015	14.2	0.26	0.019	19.7	0.24	0.012	41.2	0.25	0.006	29.8	0.27	0.009	22.4	0.28	0.013
8	F	21	14.2	0.22	0.016	13.9	0.23	0.017	13.7	0.22	0.017	12.2	0.25	0.020	14.6	0.23	0.016	30.5	0.24	0.008	23.0	0.22	0.010	17.1	0.25	0.014
9	F	21	13.2	0.27	0.021	13.1	0.27	0.020	13.4	0.27	0.020	11.6	0.29	0.025	14.8	0.27	0.019	25.0	0.27	0.011	19.7	0.25	0.013	18.3	0.28	0.016
10	F	22	11.3	0.22	0.020	11.2	0.24	0.021	10.9	0.22	0.020	10.2	0.24	0.024	12.8	0.22	0.017	19.2	0.23	0.012	15.6	0.21	0.014	12.0	0.26	0.022
11	M	22	14.3	0.22	0.016	13.8	0.22	0.016	15.2	0.21	0.014	13.3	0.21	0.016	15.7	0.22	0.014	23.5	0.23	0.010	29.2	0.21	0.007	15.5	0.24	0.016
12	M	23	17.1	0.17	0.010	15.9	0.18	0.011	16.3	0.18	0.011	14.9	0.19	0.013	16.4	0.18	0.011	28.6	0.17	0.006	23.9	0.19	0.008	16.6	0.20	0.012
13	M	25	13.4	0.22	0.016	12.7	0.21	0.017	11.7	0.21	0.018	11.0	0.25	0.023	13.4	0.22	0.016	18.7	0.24	0.013	18.7	0.23	0.012	14.4	0.27	0.018
14	F	36	14.8	0.24	0.016	14.1	0.25	0.017	15.5	0.25	0.016	13.6	0.26	0.019	16.8	0.26	0.015	22.4	0.25	0.012	23.4	0.25	0.011	17.9	0.28	0.015
15	F	49	12.6	0.21	0.017	12.3	0.22	0.018	12.0	0.21	0.018	10.6	0.24	0.023	13.7	0.23	0.017	20.4	0.24	0.014	16.6	0.23	0.012	15.1	0.26	0.017
16	F	50	15.6	0.22	0.014	14.8	0.23	0.016	15.9	0.24	0.015	13.3	0.27	0.020	19.4	0.22	0.012	32.8	0.23	0.007	21.5	0.23	0.011	21.4	0.26	0.012
17	F	56	18.8	0.27	0.015	18.7	0.27	0.014	18.5	0.28	0.015	15.5	0.29	0.019	20.6	0.25	0.012	33.8	0.28	0.008	24.9	0.27	0.011	22.7	0.33	0.015
18	M	59	10.4	0.21	0.020	10.8	0.21	0.020	10.4	0.23	0.022	9.9	0.25	0.025	11.7	0.21	0.018	17.0	0.22	0.013	15.7	0.23	0.015	12.4	0.26	0.020
19	M	59	15.9	0.20	0.013	13.5	0.18	0.014	14.8	0.19	0.013	12.5	0.20	0.016	16.1	0.20	0.012	23.4	0.19	0.008	17.5	0.19	0.011	16.3	0.20	0.012
20	F	61	13.7	0.20	0.014	13.4	0.21	0.016	13.1	0.21	0.016	11.8	0.21	0.018	16.2	0.20	0.012	26.4	0.20	0.008	22.1	0.20	0.009	15.9	0.22	0.014
21	M	71	14.4	0.20	0.014	12.8	0.21	0.017	12.7	0.22	0.017	12.0	0.23	0.019	15.1	0.21	0.014	22.0	0.23	0.011	17.1	0.21	0.012	17.5	0.28	0.016
All																										
Mean			14.6	0.22	0.015	13.9	0.22	0.016	14.1	0.22	0.016	12.5	0.24	0.020	15.8	0.22	0.014	26.4	0.23	0.009	21.4	0.22	0.011	16.8	0.25	0.015
SD			2.2	0.03	0.003	2.1	0.03	0.003	2.2	0.03	0.003	1.8	0.03	0.004	2.8	0.03	0.003	6.7	0.03	0.003	4.5	0.03	0.002	2.9	0.04	0.003
%COV			15.1	13.1	17.7	15.2	12.0	16.9	15.7	13.6	17.6	14.1	13.3	18.0	17.4	12.5	18.7	25.4	13.5	27.5	21.1	12.6	22.1	17.3	14.0	18.6

Values for V_T are given in mL/g, for K_1' in mL/g/min, and for k_2' in min^{-1}.